Radboud University Nijmegen

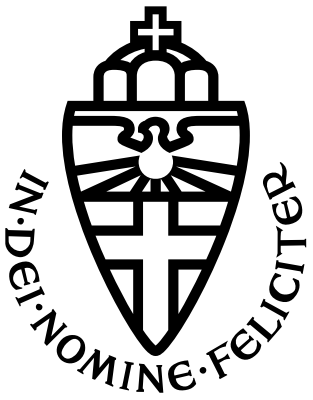

Faculty of Science

Closed photon orbits around multiple black holes

A description of null geodesics in Majumdar-Papapetrou spacetimes

Thesis BSc Physics & Astronomy

Author:
Bart Peters

Supervisor:
dr. Béatrice Bonga

Second reader:
prof. dr. Klaas Landsman

January 2021

Abstract

The first ever picture of a black hole created by the Event Horizon Telescope in April 2019 has induced new interest in research in null geodesics around black holes. While a popular topic, null geodesics around multiple black holes have not been studied extensively. In this thesis, we will look at the Majumdar-Papapetrou solution. This analytic solution describes multiple charged black holes in equilibrium and is motivated by the Schwarzschild and Reissner-Nordström solution. We will focus on closed photon orbits in particular, since most of their properties are still unknown. Moreover, for Schwarzschild and Reissner-Nordström spacetimes the properties of these special orbits are closely related to their quasinormal modes. We will provide plots of these closed photon orbits for two and three black hole spacetimes and discuss their properties such as the orbital period and stability in detail.

Contents

1 Introduction

1.1 Theory of general relativity

The most accepted theory of gravity is the theory of general relativity. It was discovered by Albert Einstein in 1915, a decade after he published his theory of special relativity. Special relativity states that the laws of physics do not depend on your frame of reference and that the speed of light in vacuum has a unique value for all observers. This theory, however, did not include the effect of gravity. In the next ten years, Einstein realised that massive objects curve time and space. The theory of general relativity was born. While Newton thought of gravity as an attractive force between masses, general relativity describes gravity as the changing geometry of space and time.

General relativity uses the concept of geodesics to describe the trajectories of free particles in spacetime. Intuitively, a geodesic is a generalisation of a straight line to a curved spacetime. It is the fastest route between two points. In this thesis we will focus on null geodesics, which are the paths travelled by photons. In a spacetime, distances can be measured by introducing the concept of a metric. A metric is a tensor which captures the geometry of the spacetime. It is the main building block of each spacetime and it can be used to derive the motion along geodesics. The underlying geometry of a spacetime does not change when one performs a coordinate transformation on a metric. Therefore, choosing a good coordinate system results in a simpler solution of the Einstein equations, which describe general relativity.

1.2 Black holes

General relativity predicts the existence of black holes. A black hole is a highly compact object, giving rise to a region in spacetime where the gravitational field is extremely strong. When matter or light gets too close to a black hole, it will end up inside it. The boundary of this region is known as the event horizon of the black hole and acts as a surface of no return.

At first these black holes were purely mathematical objects. The first solution of the Einstein equations that featured a black hole was the Schwarzschild solution. It was found in 1916 independently by Karl Schwarzschild and Johannes Droste. It describes a static spacetime, which means that the gravitational field does not change with time. The Schwarzschild black hole, which arises from this solution, is spherically symmetric and thus does not have any angular momentum.

An extension of the Schwarzschild solution is the Reissner-Nordström solution, found independently by Hans Reissner in 1916 and Gunnar Nordström in 1918. The Reissner-Nordström black hole is allowed to have an electric charge. Therefore, the gravitational field around this black hole is dependent on its mass and charge.

Both the Schwarzschild and Reissner-Nordström solution are static solutions and therefore only describe the gravitational field around a non-rotating black hole. In 1963, Roy Kerr discovered the Kerr solution, describing the gravitational field around an uncharged rotating black hole. Since the Kerr black hole is allowed to rotate, it does have angular momentum and is not spherically symmetric. In 1965, the Kerr-Newman solution was discovered. It is an extension of the Kerr solution where the black hole is allowed to have an electric charge. We will see that these two solutions are not useful for our research. Hence, they will not be discussed in further detail in this thesis.

Over the years, the existence of black holes was ratified by direct and indirect evidence. An example of indirect evidence is the accretion of matter. When matter gets close to the event horizon of a black hole, its temperature increases due to the friction which arises from the very high speed the matter has reached. Consequently, the matter converts gravitational energy into electromagnetic radiation such as light. This radiation can be observed by telescopes.

An example of more direct evidence for black holes is the detection of gravitational waves by LIGO and Virgo in 2015. Gravitational waves are small disruptions in spacetime and were predicted by general relativity. Einstein stated that these disruptions were caused by massive accelerating objects such as black holes orbiting each other. The detection of gravitational waves was another conformation that Einstein was right.

In April 2019, the team of the Event Horizon Telescope Collaboration presented the first ever picture of a black hole [2]. This was a huge breakthrough, since it is the most direct evidence for the existence of black holes and it again proves that the theory of general relativity is the best gravitational theory to date.

1.3 Multiple black hole research

The black hole picture has spurred new interest in the study of null geodesics around black holes. In contrast to single black hole spacetimes, null geodesics in spacetimes with multiple black holes have not been studied extensively. In this thesis we will look at an analytic solution which allows multiple black hole spacetimes, known as the Majumdar-Papapetrou (MP) solution. It describes a static spacetime with multiple maximally charged black holes in equilibrium. We will motivate this solution by the Schwarzschild and Reissner-Nordström solution.

We will look at two and three black hole MP spacetimes. In particular we will study closed photon orbits, since most of their properties are unknown. Some properties we will discuss in our research are the radius, orbital period and stability of orbits. In the two black hole spacetime, we will choose a cylindrical coordinate system which allows us to look at two different symmetry planes. In the three black hole spacetime, we will look at two different configurations of the black holes. We will

also compare two and three black hole spacetimes, which allows us to study how a third black hole affects the orbits around a binary.

Predicting the photon paths in multiple black hole spacetimes and studying their properties would give us more insight in light rays near black holes. However, it would be hard to compare this research with real-life observations such as the black hole picture made by the Event Horizon Telescope Collaboration. The MP spacetimes discussed in this thesis are static and thus do not allow rotating black holes. Also, by working with MP spacetimes we only consider electrically charged black holes, which have not been observed in real life (yet). Therefore the research performed in this thesis serves as a toy model for the motion of photons around multiple black holes.

2 From one to multiple black holes

2.1 Ricci & Kretschmann scalar

In this section we will discuss two curvature related scalars. These scalars are gauge-invariant and can help us gain a better understanding of the spacetime. We will start by looking at the Ricci scalar. We can determine this scalar using a direct computation, but for the spacetimes discussed in this thesis we can use a simpler argument. To this end, we solve the Einstein field equations with zero cosmological constant:

$$R_{\mu\nu} - \frac{1}{2}g_{\mu\nu}R = 8\pi T_{\mu\nu}. \tag{2.1.1}$$

In this equation $R_{\mu\nu}$ is the Ricci tensor, R is the Ricci scalar, $g_{\mu\nu}$ is the metric and $T_{\mu\nu}$ is the stress-energy tensor. The Ricci scalar is defined as $R = g^{\mu\nu}R_{\mu\nu}$, where $g^{\mu\nu}$ is the inverse metric. In order to find a direct relation between the Ricci scalar and the stress energy tensor, we can multiply Eq. (2.1.1) with the inverse metric $g^{\mu\nu}$. We find:

$$g^{\mu\nu}R_{\mu\nu} - \frac{1}{2}g^{\mu\nu}g_{\mu\nu}R = 8\pi g^{\mu\nu}T_{\mu\nu}. \tag{2.1.2}$$

Simplifying gives

$$R - \frac{1}{2}\delta^{\mu}_{\mu}R = 8\pi T^{\mu}_{\mu}. \tag{2.1.3}$$

Here, T^{μ}_{μ} is the trace of the stress-energy tensor. Using $\delta^{\mu}_{\mu} = 4$ results in

$$R = -8\pi T^{\mu}_{\mu}. \tag{2.1.4}$$

We now have derived a direct relation between the Ricci scalar and trace of the stress-energy tensor. We will see that this relation will come in handy to determine the Ricci scalar for all spacetimes discussed in this thesis.

The second curvature related scalar we will discuss is the Kretschmann scalar K. We will see that the Ricci scalar vanishes for the cases we look at. The Kretschmann scalar, on the other hand, will not. It can be determined using the Riemann tensor:

$$K = R_{\alpha\beta\gamma\delta}R^{\alpha\beta\gamma\delta}. \tag{2.1.5}$$

Since K is quadratic in the Riemann tensor, it is called a quadratic invariant. Since the Kretschmann scalar is only dependent on the Riemann tensor, it can be used to determine if a singularity in your spacetime is a coordinate singularity or a physical singularity. If the Riemann tensor is well-defined at a coordinate singularity, the Kretschmann scalar is well-defined there as well. This is not true for physical singularities, for which the Kretschmann scalar can diverge [9].

The Riemann tensor can be determined using the following equation:

$$R^{\alpha}_{\beta\gamma\delta} = \frac{\partial\Gamma^{\alpha}_{\beta\delta}}{\partial x^{\gamma}} - \frac{\partial\Gamma^{\alpha}_{\beta\gamma}}{\partial x^{\delta}} + \Gamma^{\mu}_{\beta\delta}\Gamma^{\alpha}_{\mu\gamma} - \Gamma^{\mu}_{\beta\gamma}\Gamma^{\alpha}_{\mu\delta}, \tag{2.1.6}$$

where $\Gamma^{\alpha}_{\gamma\beta}$ are the Christoffel symbols and x^{α} the coordinates of the spacetime. The Christoffel symbols can be determined using the Levi-Civita connection, to be:

$$\Gamma^{\alpha}_{\beta\gamma} = \frac{1}{2} g^{\alpha\delta} \left(\frac{\partial g_{\delta\gamma}}{\partial x^{\beta}} + \frac{\partial g_{\beta\delta}}{\partial x^{\gamma}} - \frac{\partial g_{\beta\gamma}}{\partial x^{\delta}} \right). \tag{2.1.7}$$

So after all, the Kretschmann scalar is only dependent on the metric coefficients. For the spacetimes discussed in this thesis I will make use of the Black Hole Perturbation Toolkit for Wolfram Mathematica 12.1 to determine the Kretschmann scalar [1].

2.2 Schwarzschild solution

We will now discuss different solutions of the Einstein field equations. We start by looking at a simple single black hole solution, which is known as the Schwarzschild solution. This solution is named after Karl Schwarzschild. He produced this solution in 1916, a year after Einstein stated his theory of general relativity. At the same time, Johannes Droste found this solution as well.

After studying this simple case for a single black hole, we can then advance to a more complicated solution for multiple black hole spacetimes. Since the Schwarzschild solution has been extensively studied before, we will only go through some properties which are of interest regarding our multiple black hole research.

The Schwarzschild metric in spherical coordinates is given by

$$ds^2 = -\left(1 - \frac{2GM}{c^2 r}\right) c^2 dt^2 + \left(1 - \frac{2GM}{c^2 r}\right)^{-1} dr^2 + r^2 d\theta^2 + r^2 \sin^2\theta d\phi^2. \tag{2.2.1}$$

From this point we will use geometric units, which means that we will set the speed of light c and the gravitational constant G to a value of 1. The black hole that arises from this metric is known as the Schwarzschild black hole. The only free parameter in this spacetime is the mass M. This means one can only distinguish two Schwarzschild black holes by their mass.

The Schwarzschild solution is relatively simple because it is based on some assumptions. First, the spacetime is static. This means that the gravitational field does not change with time. We can conclude this by looking at the metric coefficients, since none of the coefficients is dependent on the time coordinate t. By introducing Killing vectors in section 2.5, we will see that a static spacetime leads to conservation of the energy E of particles along their geodesic. Since we only look at null geodesics, this is the energy of the photons along their geodesic. Second, the spacetime is spherically symmetric. Using the theory of Killing vectors, this implies that the angular momentum L is conserved along the geodesics. Finally, the Schwarzschild black hole is not electrically charged.

The Schwarzschild metric (2.2.1) gives rise to two singularities. We have a physical singularity at $r = 0$ and a coordinate singularity at $r = 2M$. This coordinate singularity can be removed by switching to another coordinate system. In our spherical

coordinate system, the radius $r = 2M$ is known as the event horizon, the surface of no return.

The Schwarzschild solution is a vacuum solution, which means that the stress-energy tensor $T_{\mu\nu}$ vanishes. In particular, the stress-energy tensor is traceless. Therefore, by making use of Eq. (2.1.4), the Ricci scalar vanishes as well. But if $R = 0$ and $T_{\mu\nu} = 0$, then Eq. (2.1.1) reduces to $R_{\mu\nu} = 0$. However, this does not imply that the Riemann tensor $R_{\alpha\beta\gamma\delta}$ vanishes. Using Eq. (2.1.5) we find:

$$K = \frac{48M^2}{r^6}. \tag{2.2.2}$$

From this we can conclude that $r = 0$ is indeed a physical singularity and $r = 2M$ is a removable singularity [9].

In order to determine the photon paths around a Schwarzschild black hole, we first have to determine the equations of motion of a photon propagating in the Schwarzschild spacetime. For a detailed description of null geodesics in this spacetime, see reference [11].

Figure 1 shows the null geodesics around a Schwarzschild black hole, displayed as blue lines. The photons are coming from below, horizontally separated by a distance $1M$. The black circle corresponds to the area inside the event horizon. When photons come too close to the black hole, they will end up inside it. The radius of the grey circle is known as the photon ring. The photon ring is the only circular orbit for photons around this black hole. It has a radius of $r = 3M$ and is known to be unstable. This means that a small perturbation results in the photon exiting the orbit. It will then either escape to infinity or fall into the black hole.

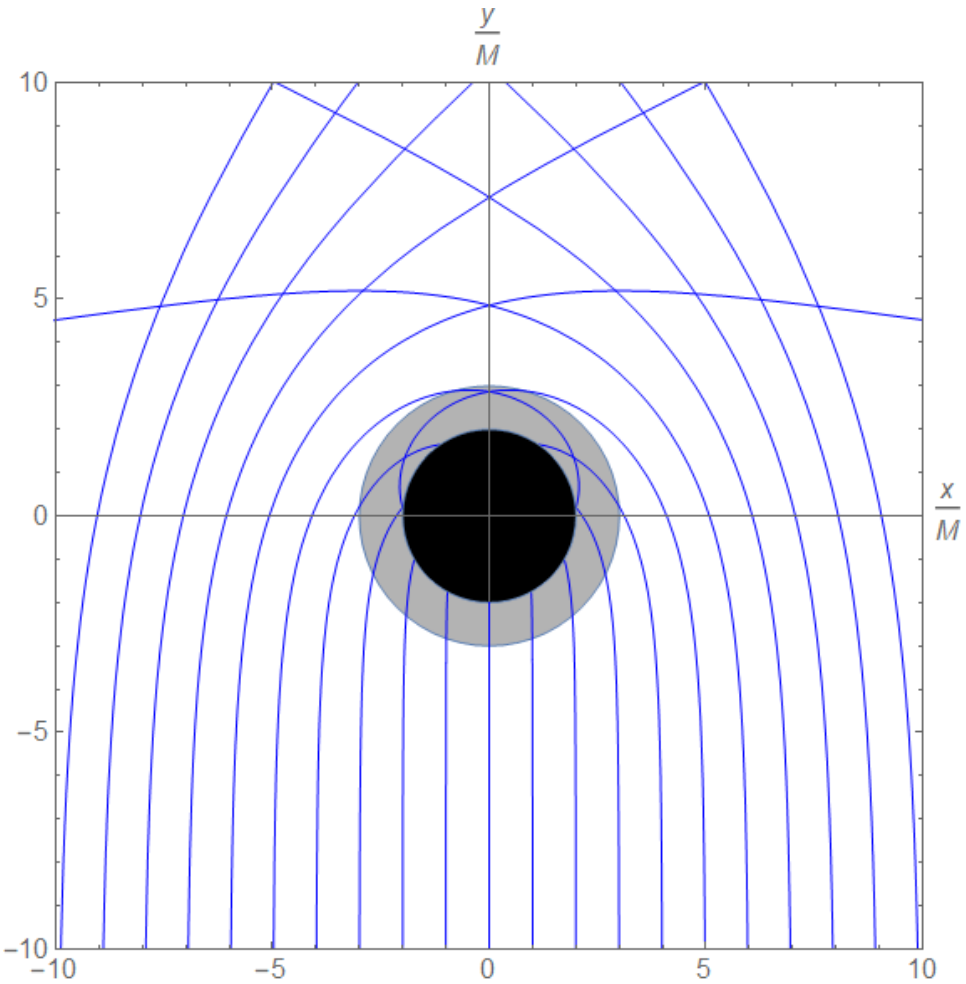

Figure 1: A two-dimensional plot of null geodesics around a Schwarzschild black hole. The null geodesics (in blue) are initially separated by a distance $1M$ in the x-direction. The black circle corresponds to the area inside the event horizon. The grey circle corresponds to the area inside the photon ring. On the axes we have Cartesian coordinates given by $x = r\cos\phi$ and $y = r\sin\phi$. The photons were shot from below with initial velocities $(v_{x_i},v_{y_i}) = (0.0,1.0)$ at a vertical initial position $y_i = -100M$.

2.3 Reissner-Nordström solution

An extension of the Schwarzschild solution is the Reissner-Nordström solution. In this solution the black hole is allowed to have an electric charge Q. This results in an extra term in the metric, which is now given by

$$ds^2 = -\left(1 - \frac{2M}{r} + \frac{Q^2}{r^2}\right)dt^2 + \left(1 - \frac{2M}{r} + \frac{Q^2}{r^2}\right)^{-1} dr^2 + r^2 d\theta^2 + r^2 \sin^2\theta d\phi^2. \quad (2.3.1)$$

The black hole which arises from this metric is known as the Reissner-Nordström black hole. Since the term concerning the electric charge is proportional to $1/r^2$, the Reissner-Nordström black hole is well approximated by the Schwarzschild black hole at large distances ($r \gg 0$).

The Reissner-Nordström solution is not a vacuum solution, but still has a vanishing Ricci scalar. The Kretschmann scalar is given by

$$K = \frac{8(7Q^4 - 12MQ^2r + 6M^2r^2)}{r^8}. \quad (2.3.2)$$

We can conclude that there is a physical singularity at $r = 0$. If we want to determine the horizons of the Reissner-Nordström black hole, we have to search for which values of r the metric components diverge. This means that we have to solve the following equation:

$$1 - \frac{2M}{r} + \frac{Q^2}{r^2} = 0. \quad (2.3.3)$$

This equation is quadratic in r. Therefore there are two solutions for the radius:

$$r = M \pm \sqrt{M^2 - Q^2}. \quad (2.3.4)$$

Since we now have two free parameters, the mass M and the charge Q, there are in general three configurations. For our research we ignore the cases $Q < M$ and $Q > M$. We are only interested in the case $Q = M$, the so called extremal case. If we substitute this relation in Eq. (2.3.4) we see that we only obtain one horizon with $r = M$. By substituting $Q = M$ in the metric (2.3.1) we obtain the metric for the extremal Reissner-Nordström black hole:

$$ds^2 = -\left(1 - \frac{M}{r}\right)^2 dt^2 + \left(1 - \frac{M}{r}\right)^{-2} dr^2 + r^2 d\theta^2 + r^2 \sin^2\theta d\phi^2. \quad (2.3.5)$$

In this metric, we have written the first two metric components as squares. The extremal Reissner-Nordström black hole with the metric as defined in (2.3.5) happens to be a good foundation for a spacetime with multiple charged black holes.

2.4 Majumdar-Papapetrou solution

Another exact solution of the Einstein field equations is the Majumdar-Papapetrou (MP) solution. This solution allows us to look at a spacetime with multiple black holes. To understand the MP metric better, we switch to a different coordinate system of the extremal Reissner-Nordström metric (2.3.5). We perform the coordinate transformation $\rho = r - M$. Our metric now has the following form:

$$ds^2 = -\frac{dt^2}{U^2} + U^2(d\rho^2 + \rho^2 d\theta^2 + \rho^2 sin^2\theta d\phi^2), \tag{2.4.1}$$

where we have defined U as

$$U = 1 + \frac{M}{\rho}. \tag{2.4.2}$$

A drawback of this coordinate transformation is that we can not speak of horizons anymore; the only horizon $r = M$ reduces to $\rho = 0$. Therefore we have to treat the black hole as a pointlike object now [12]. However, we also get lucky by doing the coordinate transformation. It happens to be that U is a solution of the Laplace equation:

$$\nabla^2 U = 0. \tag{2.4.3}$$

As a result, we can take take a whole collection of extremal Reissner-Nordström black holes. If we take a spacetime with N black holes, we can define U as follows:

$$U = 1 + \sum_{j=1}^{N} \frac{M_j}{|\mathbf{r} - \mathbf{r}_j|}. \tag{2.4.4}$$

In this definition, we sum over the mass M_j and the coordinates $\mathbf{r}_j$ of each black hole. The only change in the metric (2.4.1) is the functional form of U. If we look at a single black hole, we take $N = 1$ and we see that the definition of U in (2.4.4) reduces to U as defined in (2.4.2) with position $\mathbf{r}_j = \mathbf{0}$ [6].

Just as the Reissner-Nordström solution, the MP solution is an electrovacuum solution. This means that the MP metric satisfies the Einstein-Maxwell equations. Therefore the stress-energy tensor will be traceless. Using Eq. (2.1.4), the Ricci scalar R will vanish for all MP spacetimes.

2.5 Equations of motion

Our goal is to determine the equations of motion of photons propagating in the MP spacetimes. After we have derived these, it is possible to study the photon paths in various multiple black hole planes. In this section, we will derive the equations of motion for a spacetime in cylindrical coordinates, since we use this set of coordinates for most of our results. The cylindrical MP metric is defined as

$$ds^2 = -\frac{dt^2}{U^2} + U^2(d\rho^2 + \rho^2 d\phi^2 + dz^2), \tag{2.5.1}$$

with U a function of ρ, ϕ and z, satisfying Eq. (2.4.3). MP spacetimes are static, since the metric coefficients are time independent. In terms of general relativity, this gives rise to a so called Killing vector K^μ. If the metric is moved a little bit by K^μ and the metric doesn't change, then K^μ is a Killing vector. By using these Killing vectors we can determine the conserved quantities along the geodesic. If K^μ is a Killing vector we therefore can use

$$K_\mu \dot{x}^\mu = \text{constant}. \tag{2.5.2}$$

The dot-notation refers to the derivative of the coordinate x^μ with respect to some affine parameter λ along the geodesic:

$$\dot{x}^\mu = \frac{dx^\mu}{d\lambda}. \tag{2.5.3}$$

Because of our static spacetime we thus have a timelike Killing vector for the MP metric as defined in (2.5.1):

$$K^\mu = (1, 0, 0, 0). \tag{2.5.4}$$

We can substitute this Killing vector in Eq. (2.5.2) and we obtain out first conserved quantity:

$$\frac{\dot{t}}{U^2} = \text{constant} = E. \tag{2.5.5}$$

Here, E is the energy of the particles (or photons) along the geodesic, as already mentioned in section 2.2. A static spacetime thus results in conservation of the energy E along geodesics. Because the cylindrical MP metric (2.5.1) also is axially symmetric, we have a second Killing vector as well:

$$K^\mu = (0, 0, 1, 0). \tag{2.5.6}$$

By substituting this Killing vector in Eq. (2.5.2) we obtain our second conserved quantity:

$$\rho^2 U^2 \dot{\phi} = \text{constant} = L. \tag{2.5.7}$$

Here, L is the angular momentum. This means that in any axially symmetric system, the angular momentum L is conserved. Hence, we now have the equations of motion for the time coordinate t, Eq. (2.5.5), and for the angular coordinate ϕ, Eq. (2.5.7).

There are two approaches to determine the other equations of motion. The first approach is to use the geodesic equation:

$$\ddot{x}^\alpha + \Gamma^\alpha_{\beta\gamma}\dot{x}^\beta\dot{x}^\gamma = 0, \tag{2.5.8}$$

where $\Gamma^\alpha_{\gamma\beta}$ are the Christoffel symbols. This approach is rather time-consuming, since you have to determine all the possible Christoffel symbols using Eq. (2.1.7). More importantly, you will obtain second order differential equations using this approach.

Ideally we would like to get first order differential equations only, since they are easier to solve numerically. Therefore we will use another approach, which we will call the hybrid Lagrangian-Hamiltonian approach. We will use the Lagrangian for free particles, which is defined as

$$\mathcal{L} = \frac{1}{2}g_{\alpha\beta}\dot{x}^\alpha\dot{x}^\beta = -\frac{1}{2}\epsilon. \tag{2.5.9}$$

The constant ϵ is the norm of the vector tangent to the geodesic and is conserved. It can be seen as a normalisation condition. For null geodesics, $\epsilon = 0$.

By substituting the metric coefficients of the cylindrical MP metric (2.5.1) into Eq. (2.5.9) we can write the Lagrangian as

$$\mathcal{L} = \frac{1}{2}\left(-\frac{\dot{t}^2}{U^2} + U^2(\dot{\rho}^2 + \rho^2\dot{\phi}^2 + \dot{z}^2)\right). \tag{2.5.10}$$

We now can substitute the conserved quantities E and L as well, using Eq. (2.5.5) and Eq. (2.5.7). Therefore the Lagrangian becomes

$$\mathcal{L} = \frac{1}{2}U^2\left(-E^2 + \dot{\rho}^2 + \frac{L^2}{\rho^2U^4} + \dot{z}^2\right). \tag{2.5.11}$$

If we now use $\epsilon = 0$, we obtain the energy relation

$$E^2 = \dot{\rho}^2 + \dot{z}^2 + V_{\text{eff}}(\rho, z), \tag{2.5.12}$$

where we have defined the effective potential

$$V_{\text{eff}}(\rho, z) = \frac{L^2}{\rho^2U^4}. \tag{2.5.13}$$

We will now use the Euler-Lagrange equations to determine the other equations of motion:

$$\frac{d}{d\lambda}\left(\frac{\partial\mathcal{L}}{\partial\dot{x}^\mu}\right) = \frac{\partial\mathcal{L}}{\partial x^\mu}. \tag{2.5.14}$$

In order to obtain first-order differential equations only, we use the definition of the momentum p_μ of the coordinates:

$$p_\mu = \frac{\partial\mathcal{L}}{\partial\dot{x}^\mu}. \tag{2.5.15}$$

For the momentum in the ρ-direction we then obtain

$$p_\rho = \frac{\partial \mathcal{L}}{\partial \dot{\rho}} = U^2 \dot{\rho}. \tag{2.5.16}$$

For the momentum in the z-direction we get

$$p_z = \frac{\partial \mathcal{L}}{\partial \dot{z}} = U^2 \dot{z}. \tag{2.5.17}$$

The derivative of the momentum can easily be determined by using the Euler-Lagrange equations:

$$\dot{p}_\mu = \frac{d}{d\lambda}(p_\mu) = \frac{d}{d\lambda}\left(\frac{\partial \mathcal{L}}{\partial \dot{x}^\mu}\right) = \frac{\partial \mathcal{L}}{\partial x^\mu}. \tag{2.5.18}$$

For the derivative of the momentum in the ρ-direction this results in

$$\dot{p}_\rho = \frac{\partial \mathcal{L}}{\partial \rho} = \frac{1}{U^3}\frac{\partial U}{\partial \rho}\dot{t}^2 + U\frac{\partial U}{\partial \rho}\dot{\rho}^2 + \left(\rho^2 U \frac{\partial U}{\partial \rho} + \rho U^2\right)\dot{\phi}^2 + U\frac{\partial U}{\partial \rho}\dot{z}^2. \tag{2.5.19}$$

In a similar way, we obtain the derivative of the momentum in the z-direction:

$$\dot{p}_z = \frac{\partial \mathcal{L}}{\partial z} = \frac{1}{U^3}\frac{\partial U}{\partial z}\dot{t}^2 + U\frac{\partial U}{\partial z}\dot{\rho}^2 + \rho^2 U\frac{\partial U}{\partial z}\dot{\phi}^2 + U\frac{\partial U}{\partial z}\dot{z}^2. \tag{2.5.20}$$

In order to derive these equations we have used that $U = U(\rho, z)$. Since the metric components are functions of U^2, we also used the chain rule in these derivations: $\frac{\partial}{\partial \rho}U^2 = 2U\frac{\partial U}{\partial \rho}$ and $\frac{\partial}{\partial z}U^2 = 2U\frac{\partial U}{\partial z}$.

We can simplify the expressions of $\dot{p}_\rho$ and $\dot{p}_z$ by substituting the conserved quantities (Eq. (2.5.5) & Eq. (2.5.7)) and the momenta (Eq. (2.5.16) & Eq. (2.5.17)) into Eq. (2.5.19) & Eq. (2.5.20). By doing this we complete our system of equations of motion, which is now given by

$$\dot{t} = EU^2 \tag{2.5.21a}$$

$$\dot{\phi} = \frac{L}{\rho^2 U^2} \tag{2.5.21b}$$

$$\dot{\rho} = \frac{p_\rho}{U^2} \tag{2.5.21c}$$

$$\dot{p}_\rho = \frac{1}{U^3}\left(\left(E^2U^4 + p_\rho^2 + \frac{L^2}{\rho^2} + p_z^2\right)\frac{\partial U}{\partial \rho} + \frac{L^2 U}{\rho^3}\right) \tag{2.5.21d}$$

$$\dot{z} = \frac{p_z}{U^2} \tag{2.5.21e}$$

$$\dot{p}_z = \frac{1}{U^3}\left(E^2U^4 + p_\rho^2 + \frac{L^2}{\rho^2} + p_z^2\right)\frac{\partial U}{\partial z}. \tag{2.5.21f}$$

This system of first order differential equations can be used to study null geodesics in any MP spacetime. The structure of these differential equations stays the same when switching to a spacetime with a different number of black holes, since this only changes the functional form of U.

3 Two black holes

The first MP spacetime we are going to look at is a scenario involving two black holes. We use a cylindrical coordinate system and the metric as defined in Eq. (2.5.1). Both black holes have equal mass M and are symmetrically placed on the z-axis at $z = \pm a$. Here, a is the separation constant. Consequently, the distance between both black holes is $2a$ in this binary system. Using Eq. (2.4.4) we can define U in the following way:

$$U = 1 + \frac{M}{\sqrt{\rho^2 + (z-a)^2}} + \frac{M}{\sqrt{\rho^2 + (z+a)^2}}. \tag{3.0.1}$$

The easiest planes to study null geodesics are the symmetry planes. For this binary system we look at two of them. We start by looking at the meridian ($\phi = 0$) plane and then proceed to the plane where we have set $z = 0$. Also, we will restrict ourselves to the study of *closed* photon orbits. These particular types of null geodesics are very interesting since their properties are closely related to the (in)stability of MP spacetimes and the onset of chaos.

3.1 Meridian plane

Fixing the azimuth angle ϕ gives rise to a symmetry plane. Since we have conservation of angular momentum L, the value of ϕ can be chosen arbitrarily. Therefore we choose $\phi = 0$, and we will call this symmetry plane the meridian plane. As a result we do not have angular momentum. This follows from the second equation of motion, Eq. (2.5.21b).

Figure 2 shows a contour plot of the Kretschmann scalar for the black hole binary in the meridian plane. The spacetime is characterized by a separation constant of $a = 10M$. From the plot we can conclude that the spacetime is more strongly curved closer to each black hole.

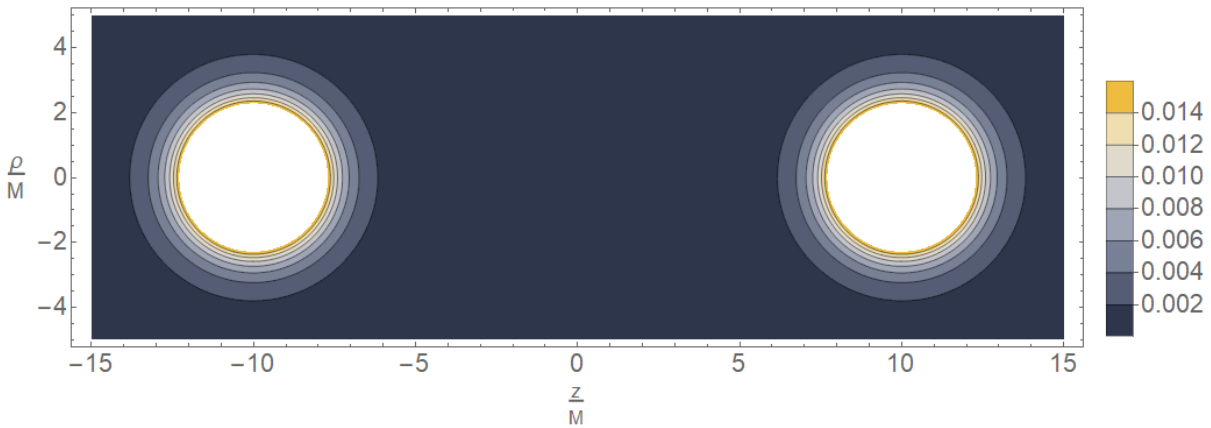

Figure 2: A contour plot of the Kretschmann scalar in the two black hole meridian plane. The distance between both holes is $20M$.

Figure 3 shows the closed photon orbits around a binary system with separation constant $a = 10M$. This plot was made by integrating the equations of motion (2.5.21) using the RK4 numerical integrator from Wolfram Mathematica 12.1. There are only three different types of closed photon orbits, which can be easily distinguished in the plot. There are two orbits which only cover one black hole each. They are shown in red and are roughly circular. There is also an orbit which covers both horizons, shown in blue. At last there is the black orbit, which we will call the 8-shaped orbit. These orbits will now be discussed in more detail.

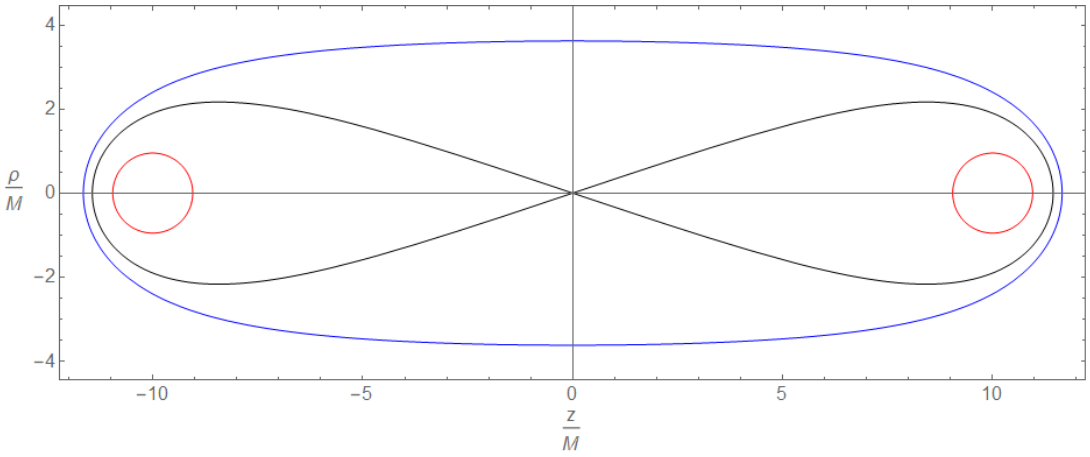

Figure 3: The only three different types of closed photon orbits around a binary system in the meridian plane, characterized by a separation constant $a = 10M$. There are two orbits which only enclose one black hole each, shown in red. These orbits are almost perfectly circular. There is an orbit which covers both black holes, shown in blue, and there is an 8-shaped orbit, shown in black.

3.1.1 Circular orbits

At first we take a closer look at the red orbits. These orbits have initial coordinates $(\rho_0,z_0) = (0, \pm 10.9543895M)$ and initial momenta $(p_{\rho_0},p_{z_0}) = (EU_0^2, 0)$. We keep the energy constant at $E = 1$ and U_0 can be determined by substituting the initial coordinates ρ_0 and z_0 into Eq. (3.0.1). The orbital period T of the orbits can be determined by integrating Eq. (2.5.21a) with respect to the affine parameter λ:

$$T = \int_0^{\lambda_{max}} \dot{t} d\lambda = E \int_0^{\lambda_{max}} U^2 d\lambda. \tag{3.1.1}$$

In this equation, λ_{max} is the value of λ when the photon has completed exactly one orbit. Numerical integration leads to $T = 26.390M$ for the red orbits with $\lambda_{max} = 5.9834$.

In Figure 3, we can see that the radii of the red orbits are approximately equal to $1M$. We can define $r = \sqrt{\rho^2 + (z \pm a)^2}$ as the radius of these circular orbits. For $\rho = 0$ we find $r = 0.9544M$. Unfortunately the red orbits are not perfectly circular. If the photon is orbiting one black hole, the distance to the other black hole will

change as the affine parameter λ increases. This means that the gravitational field of the second black hole felt by the photon will change as well. In other words, the gravitational pull from the second black hole on the photon is not constant. This results in the red orbits not being perfectly circular.

We can do a further analysis regarding the radius. By using Taylor expansions for large separations $a \gg M$ we can approximate the radius. A detailed description can be found in Appendix A.1. This leads to the following relation between the radius r and the separation constant a:

$$\frac{r}{M} \simeq 1 - \frac{M}{2a}. \tag{3.1.2}$$

Substituting $a = 10M$ results in an approximated radius of $r \simeq 0.95M$, which slightly underestimates the numerical value $r = 0.9544M$. In a similar way we can approximate the orbital period T:

$$\frac{T}{M} \simeq 8\pi\Big(1 + \frac{M}{2a}\Big). \tag{3.1.3}$$

Here we used the techniques from Appendix A.2. Substituting $a = 10M$ in this relation results in an orbital period of $T \simeq 26.389M$ for the red orbits, which is an excellent approximation to the numerical value $T = 26.390M$.

Taking the limit $a \to \infty$ in Eq. (3.1.2) results in a radius of $r = 1M$. In this case, the orbiting photon only feels the gravitational field of one black hole. The properties of a binary system with a small separation $a \ll M$ are similar to the $a = 0$ case. In this case the two black holes will unite into one black holes with twice the mass, as can be concluded from substituting $a = 0$ into Eq. (3.0.1). There will only be one orbit left. This orbit is circular and has a radius of $r = 2M$ [4].

3.1.2 The outer orbit

Next we will take a closer look at the outer (blue) orbit. It has initial coordinates $(\rho_0,z_0) = (0, \pm 11.6554316M)$ and initial momenta $(p_{\rho_0},p_{z_0}) = (EU_0^2, 0)$. Again, U_0 can be determined by substituting the initial coordinates in Eq. (3.0.1). Note that this U_0 is not equal for each orbit, since the initial coordinates vary. The orbital period can again be determined by numerically integrating Eq. (3.1.1) with $\lambda_{max} = 52.8725$. As a result we find an orbital period of $T = 95.470M$.

We observe that the radius of the outer orbit is not constant and thus a circular approximation of this orbit fails. However, we can try to find a suitable approximation for this orbit and see if we can extract useful information about the orbital period.

We first make the comparison with an elliptic orbit. We choose to have equal intersections with the axes for the ellipse and the blue orbit. Figure 4 shows a

comparison between the outer orbit (blue) and the ellipse (red). The focal points of the ellipse can be calculated using the following property of elliptic orbits:

$$z_f = \pm\sqrt{z_c^2 - \rho_c^2}. \tag{3.1.4}$$

Here, z_c and ρ_c are the coordinates of the intersection with the z- and ρ-axis respectively and are given by $(\rho_c, z_c) = (\pm 3.6198102M, \pm 11.6554316M)$. As a result we find a value of $z_f = \pm 11.0791M$. We conclude that the foci have a greater distance to the origin than the black holes. This makes sense because if we kept the foci at $z_f = \pm a$, this would result in a larger value of ρ_c based on Eq. (3.1.4).

We can now numerically integrate Eq. (3.1.1) to obtain the orbital period of the ellipse. We will make use of the parametrization $z = z_c \cos\alpha$ and $\rho = \rho_c \sin\alpha$ where $\alpha \in [0, 2\pi]$. As a result we obtain $T = 109.109M$ for the ellipse. We conclude that this value overestimates the orbital period of the blue orbit. This is consistent with Figure 4, in which we observe that the ellipse underestimates the blue orbit. Therefore the distance $\mathbf{r}$ to the origin will be smaller for the ellipse. Since U is proportional to $1/\mathbf{r}$, it will be larger for the ellipse. Since T is proportional to U^2, the ellipse has a larger value for the orbital period.

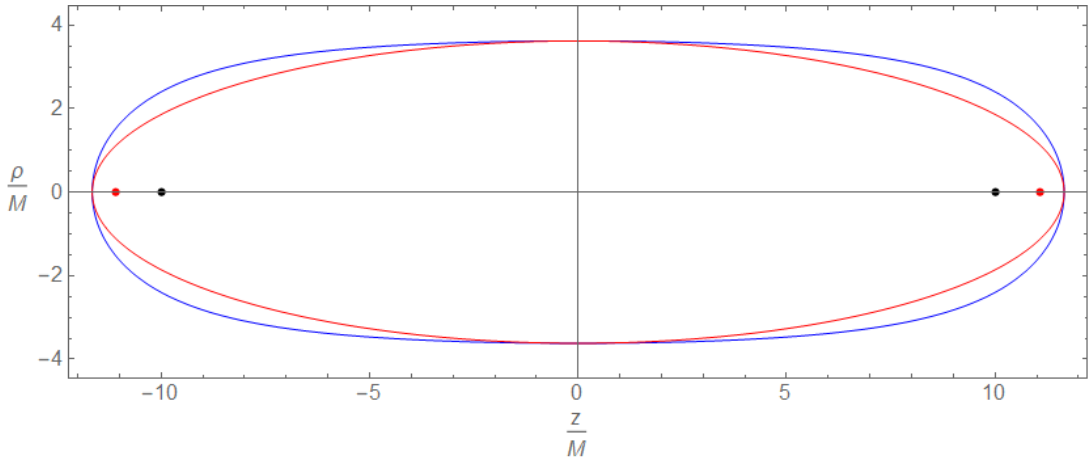

Figure 4: A direct comparison between the outer orbit of the two black hole meridian plane (blue) and its elliptic approximation (red). The intersections of both orbits with the ρ-axis and z-axis coincide. The parametrization of the ellipse is given by $z = z_c \cos\alpha$ and $\rho = \rho_c \sin\alpha$ with $\alpha \in [0, 2\pi]$. The focal points of the ellipse are given by $z_f = \pm 11.0791M$ and are shown as red dots. For clarity, the coordinates of the black holes are shown as black dots. The orbital period of the blue orbit is given by $T = 95.470M$, while the ellipse has an orbital period of $T = 109.109M$.

The ellipse is not a very good approximation of the outer orbit since it overestimates the orbital period by 14.3%. Therefore we look for a parametrization that fits the blue orbit better. This leads us to the so called extended circle approximation, shown in Figure 5.

This extended circle is characterized by two parametrizations. At first we have the straight horizontal lines, parametrized by $\rho = \pm q$ and $z \in [-d, d]$. Then there are the two halve circles. The left circle is parametrized by $z = q\cos\alpha - d$ and $\rho = q\sin\alpha$ with $\alpha \in [\frac{\pi}{2}, \frac{3\pi}{2}]$. The circle on the right is parametrized by $z = q\cos\alpha + d$ and $\rho = q\sin\alpha$ with $\alpha \in [-\frac{\pi}{2}, \frac{\pi}{2}]$. The parameter q determines the height of the extended circle and the parameter d determines the width. Both parameters are chosen such that the extended circle visually fits the blue orbit in the best way. This leads to the values $q = 3.35M$ and $d = 8.00M$.

We can again determine the orbital period by numerically integrating Eq. (3.1.1). Since our approximation yields a symmetric orbit we can integrate over one quarter of the orbit and then, at the end, multiply the obtained value by 4. Also, since we did two parametrizations, we split the integral in two parts. In one part we integrate over the horizontal line, in the other part we integrate over the circle. Performing these steps results in an orbital period of $T = 91.062M$ for the extended circle. Hence, this is a better approximation than the ellipse, since the orbital period is only underestimated by 4.8%.

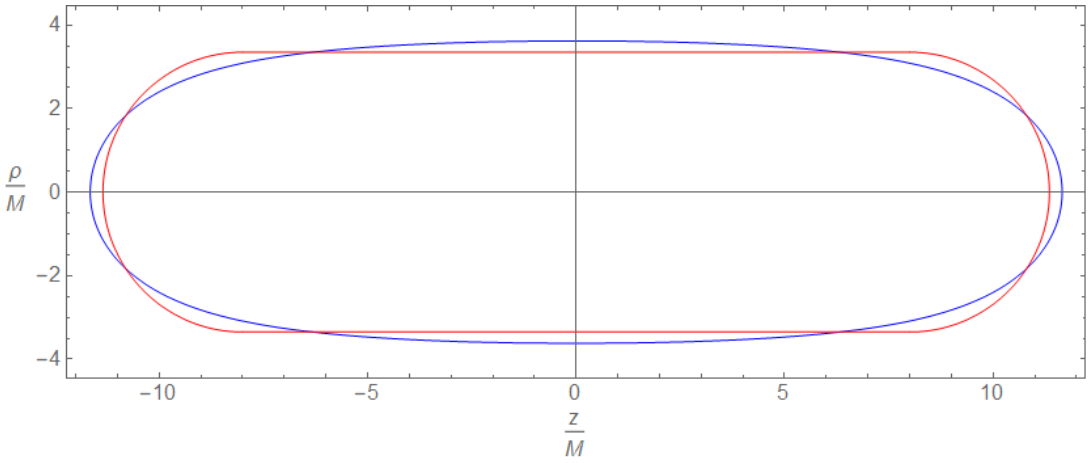

Figure 5: A direct comparison between the outer orbit of the two black hole meridian plane (blue) and its extended circle approximation (red). The straight horizontal lines are given by $\rho = \pm q$ and $z \in [-d, d]$. The circle on the left is given by $z = q\cos\alpha - d$ and $\rho = q\sin\alpha$ with $\alpha \in [\frac{\pi}{2}, \frac{3\pi}{2}]$. The right circle is parametrized by $z = q\cos\alpha + d$ and $\rho = q\sin\alpha$ with $\alpha \in [-\frac{\pi}{2}, \frac{\pi}{2}]$. The orbital period of the outer orbit is given by $T = 95.470M$, while the extended circle has an orbital period of $T = 91.062M$.

3.1.3 The 8-shaped orbit

The last closed photon orbit in the two black hole meridian plane is the black 8-shaped orbit. The photon follows an 8-like trajectory, circling between both black holes. The initial coordinates and momenta of this orbit are given by $(\rho_0, z_0) = (0, \pm 11.4414475M)$ and $(p_{\rho_0}, p_{z_0}) = (EU_0^2, 0)$, respectively. Once again, U_0 can be derived by substituting ρ_0 and z_0 in Eq. (3.0.1). Numerically integrating Eq.

(3.1.1) with $\lambda_{max} = 51.5001$ results in an orbital period of $T = 98.789M$ for the 8-shaped orbit.

This orbit does not have a simple shape such as a circle or an ellipse. Therefore, we apply the same techniques of using multiple parametrizations as in the extended circle approximation of the blue orbit to approximate this orbit. A major difference, however, is that we use three different parametrizations instead of two. The 8-shaped orbit and its approximation are shown in Figure 6.

The parametrization of the left circular part is given by $z = q\cos\alpha - d$ and $\rho = q\sin\alpha$ with $\alpha \in [\frac{\pi}{2}, \frac{3\pi}{2}]$. The right circular part is parametrized by $z = q\cos\alpha + d$ and $\rho = q\sin\alpha$ with $\alpha \in [-\frac{\pi}{2}, \frac{\pi}{2}]$. The parameter q determines the height of the approximated orbit, while d corresponds to the horizontal distance from the origin to the start of the circular parts. The semicircles are glued to horizontal lines. The left lines are parametrized by $\rho = \pm q$ and $z \in [-d, -v]$, while the right lines are given by $\rho = \pm q$ and $z \in [v, d]$. The parameter v corresponds to the horizontal distance from the origin to the beginning of the horizontal lines. Finally, these horizontal lines are connected with two diagonal lines. These diagonal parts of the approximated orbit are parametrized by $\rho = \pm\frac{q}{v}z$ and $z \in [-v, v]$. The parameters q, d and v are chosen to visually approximate the 8-shaped orbit in the best way. This leads to the values $q = 2.15M$, $d = 9.20M$ and $v = 7.06M$.

The final step will be to determine the orbital period of the approximated orbit. We will have to split the integral from Eq. (3.1.1) into three parts. Each part corresponds to a different parametrization. We will again use that the approximated orbit is symmetric. Therefore, by choosing the right boundaries for each integral, we can integrate over one fourth of the orbit and multiply our final result by 4. After performing all these steps we obtain an orbital period for the approximated orbit of $T = 99.402M$. We can conclude that this approximation works quite well, since it only overestimates the orbital period of the 8-shaped orbit by 0.6%.

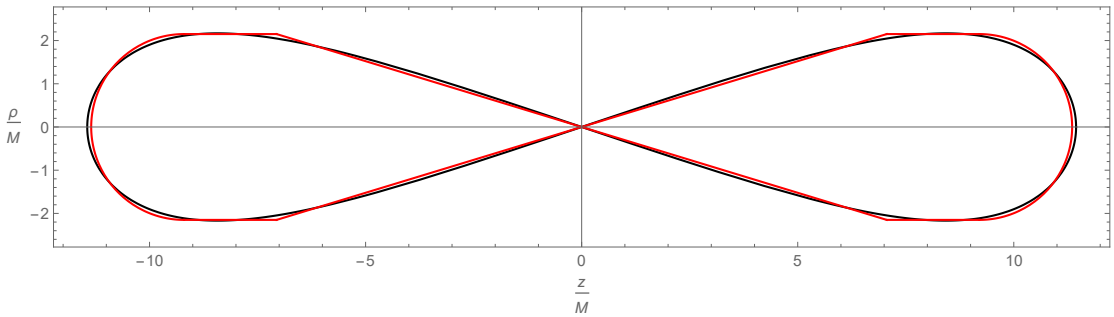

Figure 6: A direct comparison between the 8-shaped orbit of the two black hole meridian plane (black) and its approximation (red). There is made use of three kinds of parametrizations for the approximated orbit: a circle, straight horizontal lines and diagonal parts. The orbital period of the 8-shaped orbit is given by $T = 98.789M$, while its approximation has an orbital period of $T = 99.402M$.

3.2 $z = 0$ plane

We will now take a closer look at another symmetry plane in our cylindrical coordinate system where we will set the z-coordinate equal to 0. In this symmetry plane, angular momentum is allowed. The black holes are placed on the z-axis. This means their coordinates are not located in this symmetry plane. Let us first rewrite U from Eq. (3.0.1) by substituting $z = 0$. We will get:

$$U = 1 + \frac{2M}{\sqrt{\rho^2 + a^2}}. \tag{3.2.1}$$

We see that U is only dependent on ρ, which now acts as a radial coordinate in this symmetry plane. In order to highlight the strong gravitational effects, we place the two black holes closer together at $a = M/5$. In this plane it is more convenient to rescale the coordinates with a instead of M. We can now numerically solve the equations of motion from Eq. (2.5.21), where we use $z = \dot{z} = 0$.

Figure 7 shows three examples of closed photon orbits in the $z = 0$ symmetry plane for two black holes. The orbits do not have a simple shape anymore. The photon precesses with some kind of periodicity. Moreover, a small change in initial coordinates results in very different orbits.

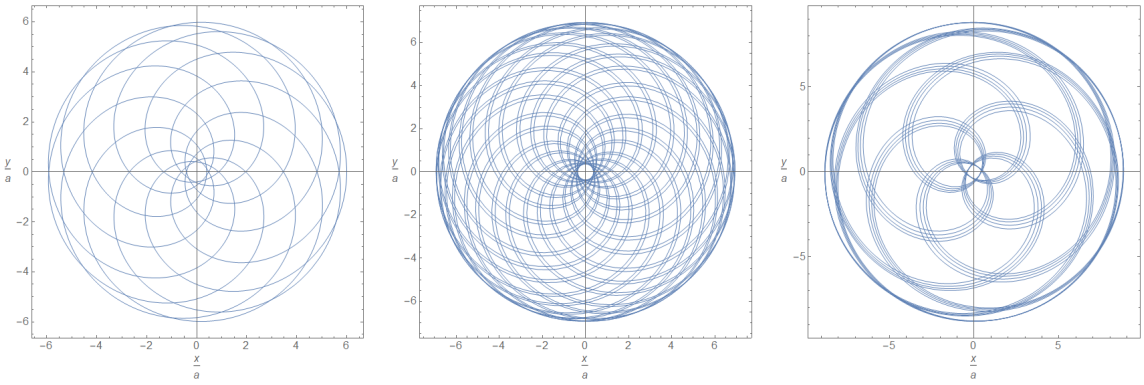

Figure 7: Three different closed photon orbits in the two black hole $z = 0$ symmetry plane. Both black holes have equal mass $M = 5a$ and are placed on the z-axis. On the axes we have Cartesian coordinates given by $x = \rho\cos\phi$ and $y = \rho\sin\phi$. From left to right, the orbits have initial coordinates $(x_0, y_0) = (6.00a, 0)$, $(x_0, y_0) = (6.94a, 0)$ and $(x_0, y_0) = (8.81a, 0)$ and values for the affine parameter $\lambda_{max} = 57.31$, $\lambda_{max} = 277.02$ and $\lambda_{max} = 235.99$. The initial velocities of all three orbits are given by $(v_{x_0}, v_{y_0}) = (0.0, 1.0)$.

Despite the difficult shapes of the orbits we can do some further analysis regarding the radial coordinate ρ and investigate if there are any circular orbits in this plane. Therefore we have to look for critical points of the effective potential from Eq.

(2.5.13). In this symmetry plane the effective potential in only dependent on the radial coordinate. To find out if there are circular orbits we have to solve

$$\frac{\partial V_{eff}}{\partial \rho} = 0. \tag{3.2.2}$$

By solving this equation for ρ we will obtain the radii of the possible circular orbits. First we substitute U from Eq. (3.2.1) into Eq. (2.5.13). Secondly we differentiate this relation with respect to the radial coordinate. Then, after setting this equal to 0 and some rearranging, we obtain the following equation:

$$2M(\rho^2 - a^2) = (\rho^2 + a^2)^{\frac{3}{2}}. \tag{3.2.3}$$

Making use of the substitution $\eta^2 = \rho^2 + a^2$ results in a cubic equation:

$$\eta^3 - 2M\eta^2 + 4Ma^2 = 0. \tag{3.2.4}$$

The discriminant of this cubic equation is given by

$$D = 128M^2a^2\Big(M^2 - \frac{27}{8}a^2\Big). \tag{3.2.5}$$

From this relation we can conclude that there are two circular orbits in the two black hole $z = 0$ plane, provided that $M^2 > \frac{27}{8}a^2$. In order to solve the cubic equation (3.2.4) we make use of a trigonometric identity [8] and find the following relations for the inner and outer circular orbit, respectively:

$$\frac{\rho_{in}}{a} = \sqrt{\frac{4M^2}{9a^2}\left(1 - 2\sin\left(\frac{\pi}{6} - \frac{1}{3}\cos^{-1}\gamma\right)\right)^2 - 1}, \tag{3.2.6}$$

$$\frac{\rho_{out}}{a} = \sqrt{\frac{4M^2}{9a^2}\left(1 + 2\cos\left(\frac{1}{3}\cos^{-1}\gamma\right)\right)^2 - 1}. \tag{3.2.7}$$

In these equations, $\gamma = 1 - \frac{27a^2}{4M^2}$. Both expressions are only valid provided that $M^2 > \frac{27}{8}a^2$ [10]. For our two black hole plane characterized by $M = 5a$, we obtain the relations $\rho_{in} = 1.167a$ and $\rho_{out} = 9.740a$.

The left part of Figure 8 shows a plot of the inner (black) and outer (red) circular orbit. The right part shows a direct comparison between a closed photon orbit (blue) and both circular orbits. A closed photon orbit is only possible if $\rho \leq \rho_{out}$, where ρ is the outer radius of the photon orbit. If this inequality does not hold, the gravitational field of both black holes is not strong enough for the photon to orbit and the photon will only get bent and escape to infinity. The closed photon orbits in Figure 7 also seem to have a small inner radius, acting as the smallest distance to the origin the photon can reach. When the outer radius ρ increases, this smaller radius will decrease.

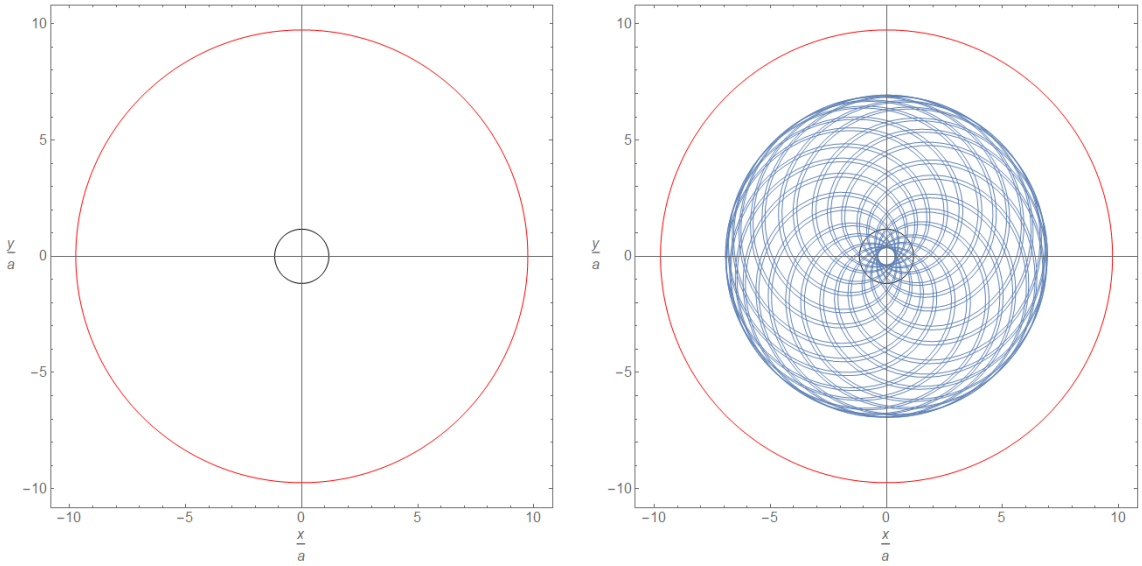

Figure 8: The only two circular orbits in the two black hole $z = 0$ plane (left plot), compared with the middle closed photon orbit from Figure 7 (right plot). The radii of the inner (black) and outer (red) circular orbits are given by $\rho_{in} = 1.167a$ and $\rho_{out} = 9.740a$, respectively. The outer circular orbit seems to be unstable, while the inner circular orbit is stable.

We can study the circular orbits in this symmetry plane in further detail by performing a stability analysis. The effective potential reaches a minimum value at $\rho = \rho_{in}$. Therefore, this orbit is stable. However, the effective potential reaches a maximum value at $\rho = \rho_{out}$ so that this orbit is unstable. A small perturbation in the radial direction $\delta\rho$ will cause the photon to exit this orbit. This $\delta\rho$ grows exponentially with time:

$$\delta\rho \sim e^{\lambda t}. \tag{3.2.8}$$

Here, λ is the Lyapunov exponent. It describes the timescale of the exponential growth. A smaller value of λ will result in a smaller exponential growth of $\delta\rho$. Consequently, the orbit will be more stable. We can analytically determine the Lyapunov exponent of the outer circular orbit and determine how its stability depends on the mass of the black holes. A full derivation of the Lyapunov exponent of the outer circular orbit is given in Appendix B. The Lyapunov exponent as a function of the mass is shown in red in Figure 9. After performing a third order Taylor expansion for $M \gg 1$ we found the following relation for λ:

$$\frac{\lambda}{a} \simeq \frac{a}{8\sqrt{2}M} - \frac{5a^3}{64\sqrt{2}M^3}. \tag{3.2.9}$$

This relation, shown in blue in Figure 9, is a good approximation of λ for large M. Therefore, we can conclude that the outer circular orbit is more stable for more massive black holes. [4]

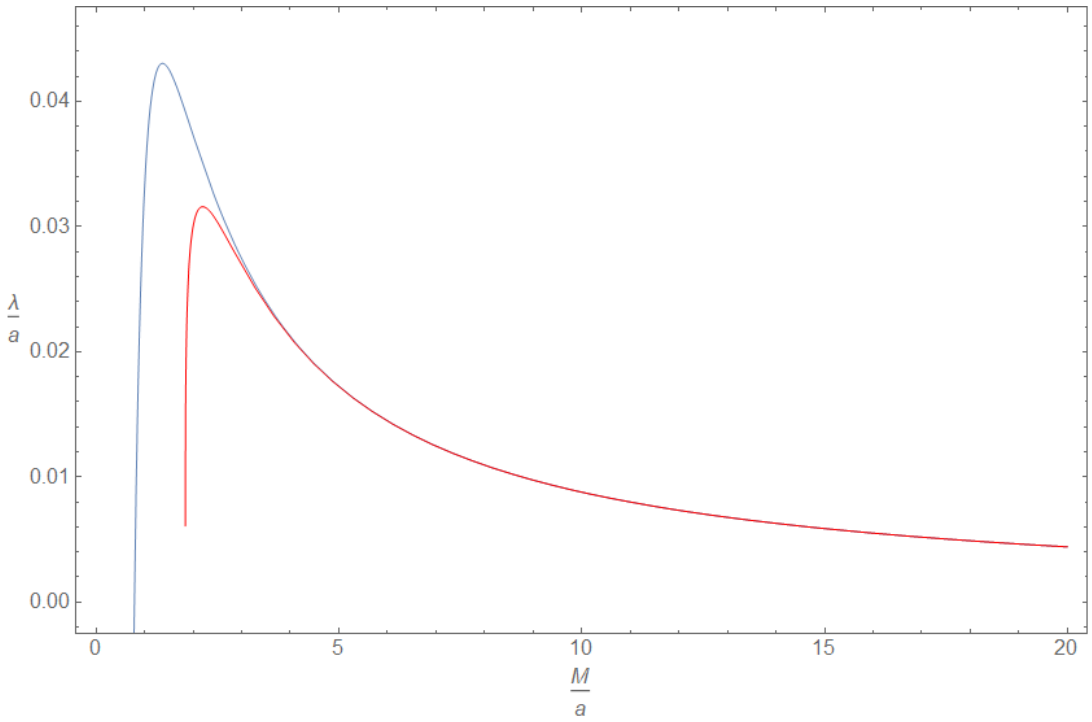

Figure 9: The Lyapunov exponent λ as a function of the mass M of the outer circular orbit in the two black hole $z = 0$ plane, shown in red. The blue curve corresponds to its third order Taylor expansion (Eq. (3.2.9)).

4 Three black holes

4.1 Cylindrical case

In this chapter we will discuss two scenarios regarding a three black hole MP spacetime. At first we will look at an extension of the two black hole meridian plane. We place three black holes on the z-axis with equal mass M and separation a. Therefore we will call this scenario the cylindrical case. We can define U as

$$U = 1 + \frac{M}{\sqrt{\rho^2 + (z-a)^2}} + \frac{M}{\sqrt{\rho^2 + z^2}} + \frac{M}{\sqrt{\rho^2 + (z+a)^2}}. \tag{4.1.1}$$

Since this configuration is also a meridian plane, photons restricted to this plane necessarily have vanishing angular momentum. A notable difference with the two black hole meridian plane is the definition of the separation constant a. In the three black hole case, the distance between the left and middle black hole as well as the distance between the middle and right black hole is equal to a. In the two black hole case, however, the distance between both black holes is $2a$.

Figure 10 shows a contour plot of the Kretschmann scalar for this cylindrical case, characterized by a separation of $a = 20M$. We observe that the spacetime is more strongly curved closer to the black holes, which is the same conclusion as we found in the two black hole meridian plane.

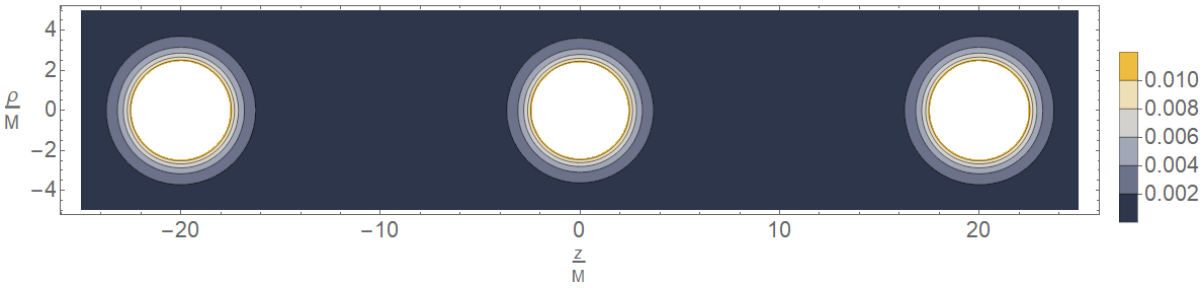

Figure 10: A contour plot of the Kretschmann scalar in the three black hole meridian plane, characterized by $a = 20M$.

Figure 11 shows all closed photon orbits for the cylindrical case with $a = 20M$. We observe that adding only one black hole results in three additional closed photon orbits. All orbits have initial coordinates $\rho_0 = 0$ and z_0 as stated in Table 1. The initial momenta are given by $p_\rho = EU_0^2$ and $p_z = 0$. The energy is given by $E = 1$ and U_0 can be determined by substituting the initial coordinates in Eq. (4.1.1). Table 1 also gives the orbital periods T of each orbit, obtained from numerically integrating Eq. (3.1.1).

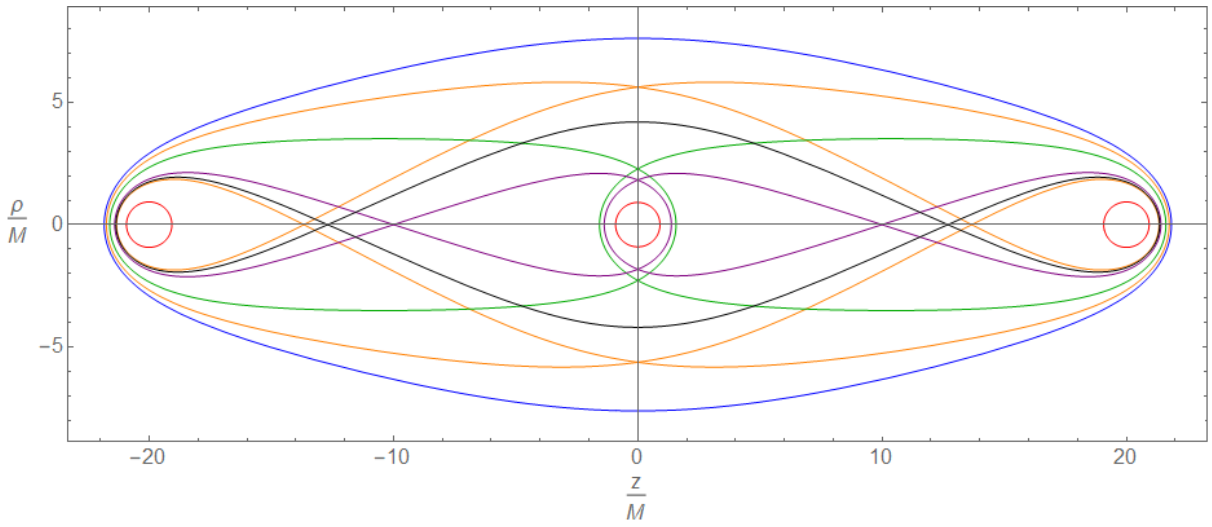

Figure 11: All different types of closed photon orbits in the three black hole meridian plane, characterized by a separation constant $a = 20M$.

Some orbits can be easily compared with the two black hole meridian plane. The green and purple orbit in Figure 11 correspond to the blue and black orbit in Figure 3, respectively. The circular orbits, shown in red in both figures, are similar as well.

Orbit(s)	z_0/M	λ_{max}	T/M
Blue	21.844147170	97.2653	160.597
Orange	±21.752703953	95.3078	168.065
Green	±21.618973331	52.4128	100.551
Purple	±21.413150389	51.1266	103.875
Black	21.362320412	94.0260	174.026
Red (outer)	±20.932594703	5.8441	27.018
Red (middle)	0.908806050	5.7107	27.647

Table 1: The initial coordinates z_0, the values of the affine parameter for one orbit λ_{max} and the orbital periods T of all orbits from Figure 11.

4.1.1 Circular orbits

From Table 1 we observe that the radius of the middle circular orbit is somewhat smaller than the radii of both outer circular orbits, which are equal. This a difference with the two black hole meridian plane, where the radii of the circular orbits were equal. In order to get a better understanding of the circular orbits, we will again use first order Taylor expansions for large separations. By making use of the techniques discussed in Appendix A.1, we find for the middle orbit:

$$\frac{r}{M} \simeq 1 - \frac{2M}{a}. \tag{4.1.2}$$

Substituting $a = 20M$ in this relation results in $r \simeq 0.9M$, which only underestimates the radius of the middle circular orbit from Figure 11 by 1.0%. We can do the same expansion for the outer circular orbits. As a result we find that both radii are equivalent and equal to

$$\frac{r}{M} \simeq 1 - \frac{3M}{2a}. \tag{4.1.3}$$

Hence, the inner circular orbit indeed has a smaller radius than the outer circular orbits. Substituting $a = 20M$ in Eq. (4.1.3) results in $r \simeq 0.9M$ for the outer circular orbits, which only underestimates the numerical value by 0.8%.

The difference in radii can also be explained in a physical way. A photon orbiting the middle black hole feels, apart from the black hole it is orbiting, the presence of two black holes at a distance a. A photon orbiting the most left or most right black hole also feels the presence of two black holes apart from it's own black hole. However, it feels one black hole at a distance a and another at a distance $2a$. As a result, the gravitational pull on a photon orbiting one of the outer black holes will be slightly smaller than the gravitational pull on a photon orbiting the middle black hole. Therefore, the photon orbiting the middle black hole has to be a little bit closer to the black hole in order to compensate the extra gravitational pull from the other two black holes.

The orbital period T of all three circular orbits can be determined by using the techniques from Appendix A.2. For the middle circular orbit we find

$$\frac{T}{M} \simeq 8\pi\Big(1 + \frac{2M}{a}\Big) \tag{4.1.4}$$

and for the outer circular orbits we get

$$\frac{T}{M} \simeq 8\pi\Big(1 + \frac{3M}{2a}\Big). \tag{4.1.5}$$

By using $a = 20M$ we find the approximated values $T \simeq 27.646M$ for the middle circular orbit and $T \simeq 27.018M$ for the outer circular orbits. By comparing these results with the orbital periods from Table 1 we can conclude that the Taylor expansion for $a \gg M$ is an excellent approximation for the orbital period.

For a separation constant of $a = 20M$ these approximations work quite well. We can vary a and see how this affects the approximations of r and T. Figure 12 and Figure 13 show r and T as a function of a for the middle circular orbit, respectively. Similar plots can be made for the outer circular orbits. As it should, the error one makes in only keeping the leading term in a/M reduces for larger a. Interestingly, at a given a the error is smaller for the orbital period T than for the radius r.

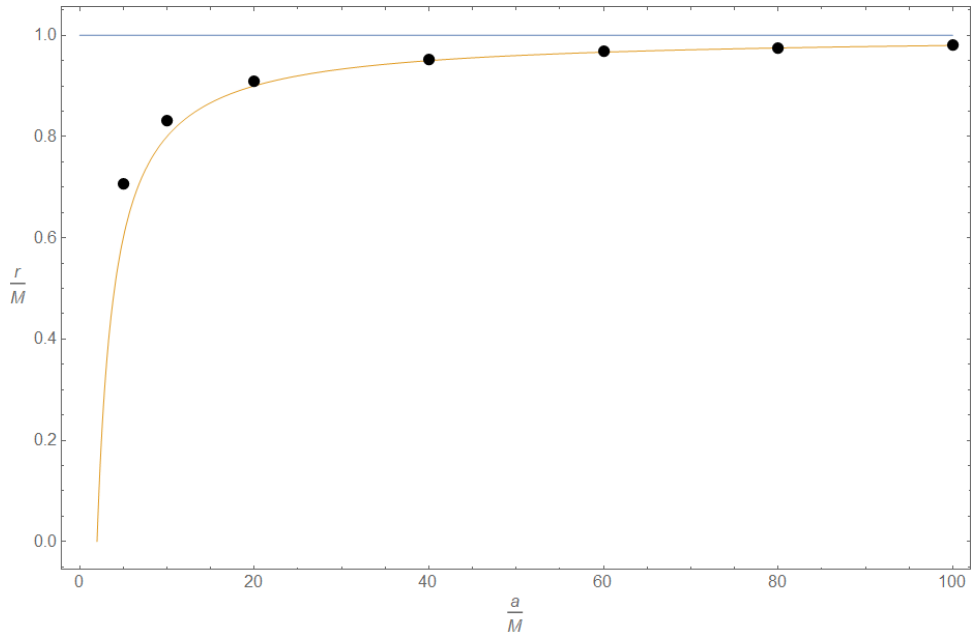

Figure 12: The radius of the middle circular orbit in the three black hole meridian plane as a function of the separation constant. The yellow line represents the Taylor expansion from Eq. (4.1.2), while the black dots are the numerical results. The blue line corresponds to the asymptotic value of $r = 1M$.

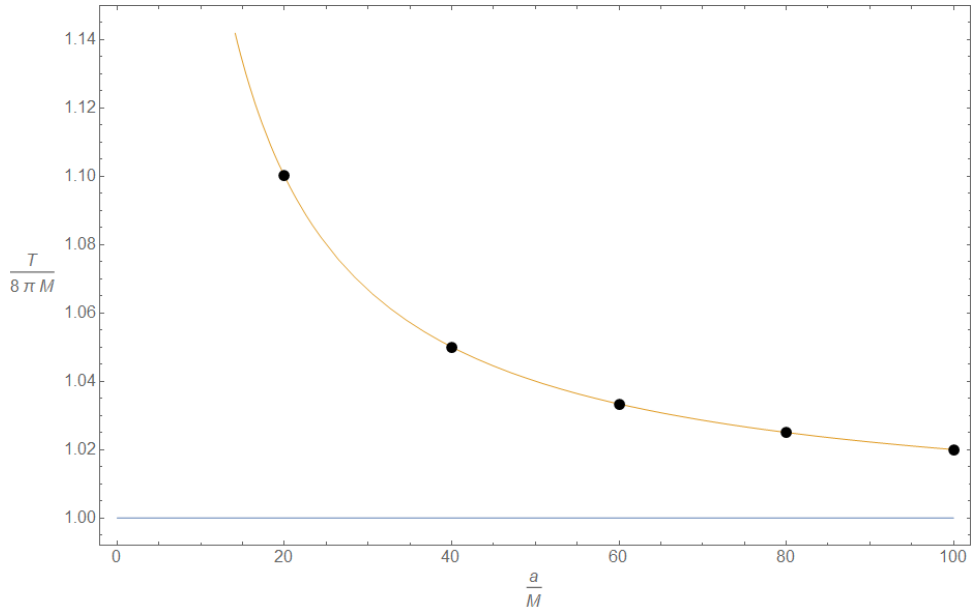

Figure 13: The orbital period of the middle circular orbit in the three black hole meridian plane as a function of the separation constant. The yellow line represents the Taylor expansion from Eq. (4.1.4), while the black dots are the numerical results. The blue line corresponds to the asymptotic value of $T = 8\pi M$.

We have now studied the radii and orbital periods of circular orbits in MP spacetimes with two and three black holes in the meridian plane in detail. Therefore, it is interesting to compare the results from both planes. In the two black hole case, the distance between the black holes is $2a$. In order to compare the radius of the circular orbits, we define $b = 2a$. Now, b measures the distance between the black holes in the two black hole scenario while a defines the separation in the three black hole case. As a result we can rewrite Eq. (3.1.2):

$$\frac{r}{M} \simeq 1 - \frac{M}{b}. \tag{4.1.6}$$

We can now compare this relation with Eq. (4.1.2) and Eq. (4.1.3). The circular orbits in the two black hole meridian plane have the biggest radii. This can again be explained in a physical way. In the two black hole case, a photon orbiting one black hole only feels the gravitational pull of one black hole at a distance b. A photon orbiting one of the black holes from the three black hole plane will always experience a bigger gravitational pull, since it feels the presence of an extra black hole.

The final property of the circular orbits in the cylindrical case we will study is their stability. We will therefore determine the Lyapunov exponent λ for the middle and outer circular orbit(s) by making use of the techniques mentioned in Appendix B. Figure 14 shows that the middle circular orbit has a slightly higher value of λ for all values of M. This means that the outer circular orbits are somewhat more stable than the middle one. For both cases λ is proportional to $1/M$, meaning that more massive black holes result in more stable circular orbits.

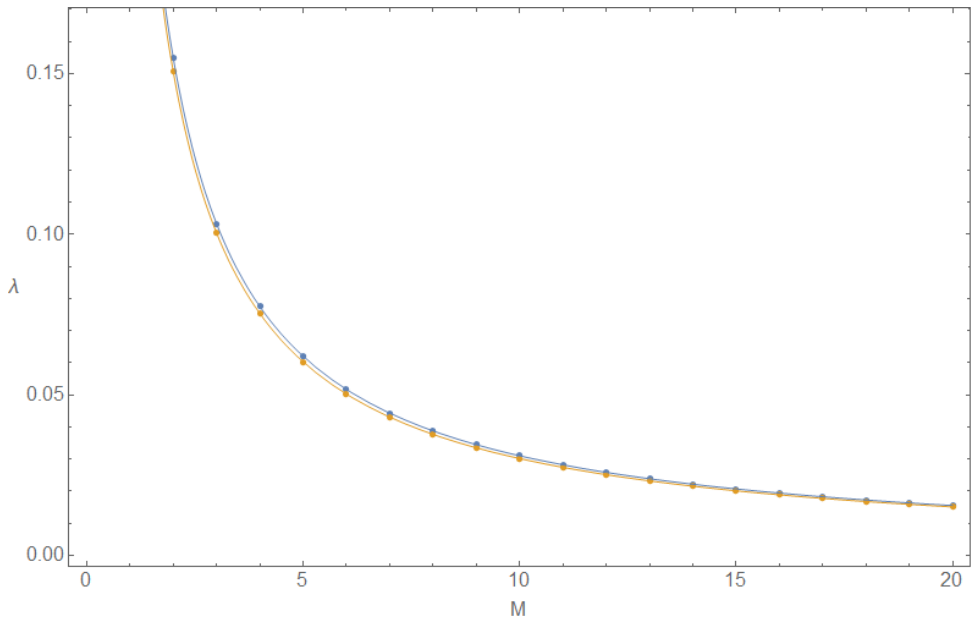

Figure 14: The Lyapunov exponent of the middle (blue) and the outer (yellow) circular orbit(s) as a function of the mass in the cylinder case, characterized by $a = 20M$. Both lines represent a fit through the values of λ, shown as dots.

4.1.2 The outer orbit

We will now have a closer look at the outer (blue) orbit of the cylindrical case. The shape of this orbit is better approximated by an ellipse than an extended circle. Using this approximation, we calculate an approximated value of the orbital period T. We will look at four of such approximations:

1. Ellipse approximation A: The area of the orbit and the ellipse are equal and the intersections with the axes are chosen such that the orbit is visually approximated in the best way. Figure 15 shows the outer orbit (blue) and ellipse A (orange).
2. Ellipse approximation B: The orbit and the ellipse have equal intersections with the axes. Figure 16 shows the outer orbit (blue) and ellipse B (red).
3. Ellipse approximation C: The focal points of the ellipse coincide with the locations of the outer black holes at $z = \pm 20M$. The intersections with the axes are chosen such that the orbit is visually approximated in the best way. Figure 17 shows the outer orbit (blue) and ellipse C (green).
4. Ellipse approximation D: The area of the orbit and the ellipse are equal. The focal points of the ellipse and the locations of the outer black holes coincide at $z = \pm 20M$. The intersections with the axes are chosen such that the orbit is visually approximated in the best way. Figure 18 shows the outer orbit (blue) and ellipse D (purple).

The focal points and the intersections with the axes are related by Eq. (3.1.4). The area of an ellipse A and the intersections with the axes are related by

$$A = \pi \rho_c z_c. \tag{4.1.7}$$

Here, ρ_c and z_c are the intersections with the ρ- and z-axis, respectively. All ellipse parametrizations are given by $\rho = \rho_c \sin\alpha$ and $z = z_c \cos\alpha$. These expressions can be substituted in Eq. (4.1.1) to obtain an approximated value of U. We substitute this value of U in Eq. (3.1.1) and after numerically integrating this expression, we obtain a value of the approximated orbital period.

All properties of the blue orbit and the ellipse approximations are given in Table 2. Ellipse B approximates the orbital period in the best way.

Orbit	A/M^2	z_f/M	ρ_c/M	z_c/M	T/M
Outer (blue)	519.747	$-$	7.62306	21.84415	160.597
Ellipse A	519.747	± 20.450	7.58500	21.81155	171.016
Ellipse B	523.136	± 20.471	7.62306	21.84415	170.437
Ellipse C	505.426	± 20	7.52841	21.37000	177.733
Ellipse D	519.747	± 20	7.71741	21.43731	175.512

Table 2: A direct comparison between some properties of the outer blue orbit from Figure 11 and its elliptic approximations. The properties which are given are the area enclosed by the orbit (A), the focal points of the ellipse (z_f), the intersection with the ρ-axis (ρ_c), the intersection with the z-axis (z_c) and the orbital period (T).

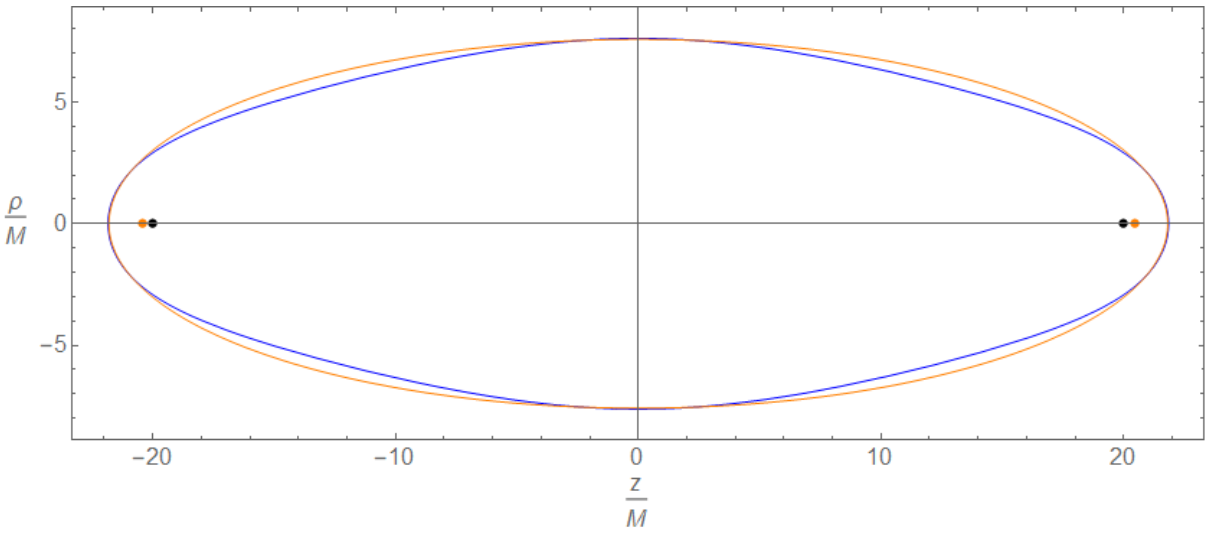

Figure 15: A direct comparison between the outer orbit in the cylinder case (blue) and ellipse A (orange). The latter is an approximation of the former, where we have chosen to have equal areas. The black dots represent the coordinates of the black holes, while the orange dots are the focal points of the ellipse.

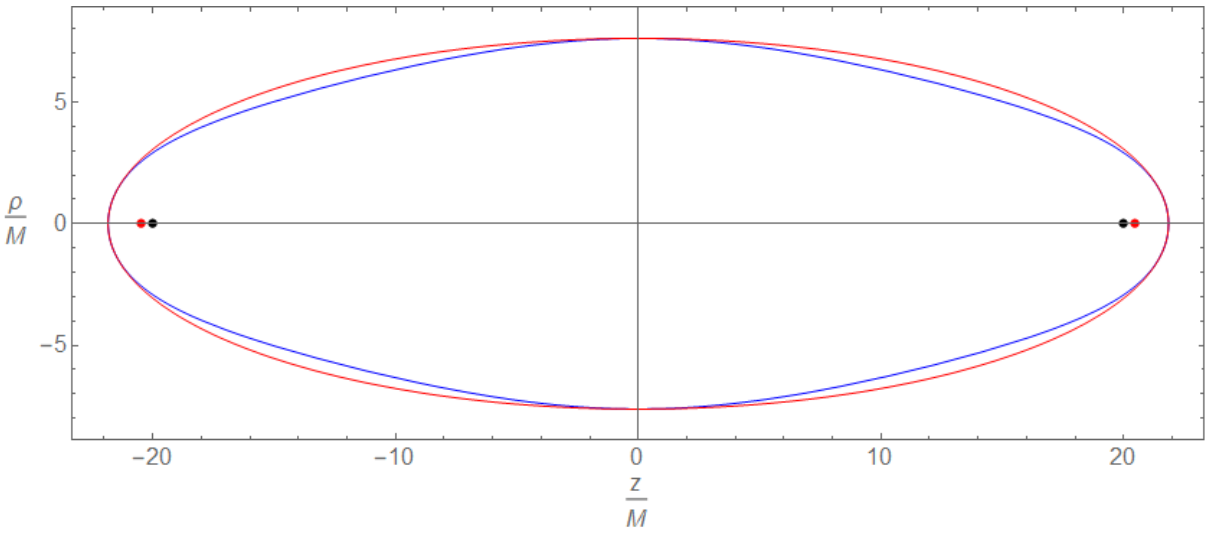

Figure 16: A direct comparison between the outer orbit in the cylinder case (blue) and ellipse B (red). The latter is an approximation of the former, where we have chosen equal intersections with the axes. The black dots represent the coordinates of the black holes, while the red dots are the focal points of the ellipse.

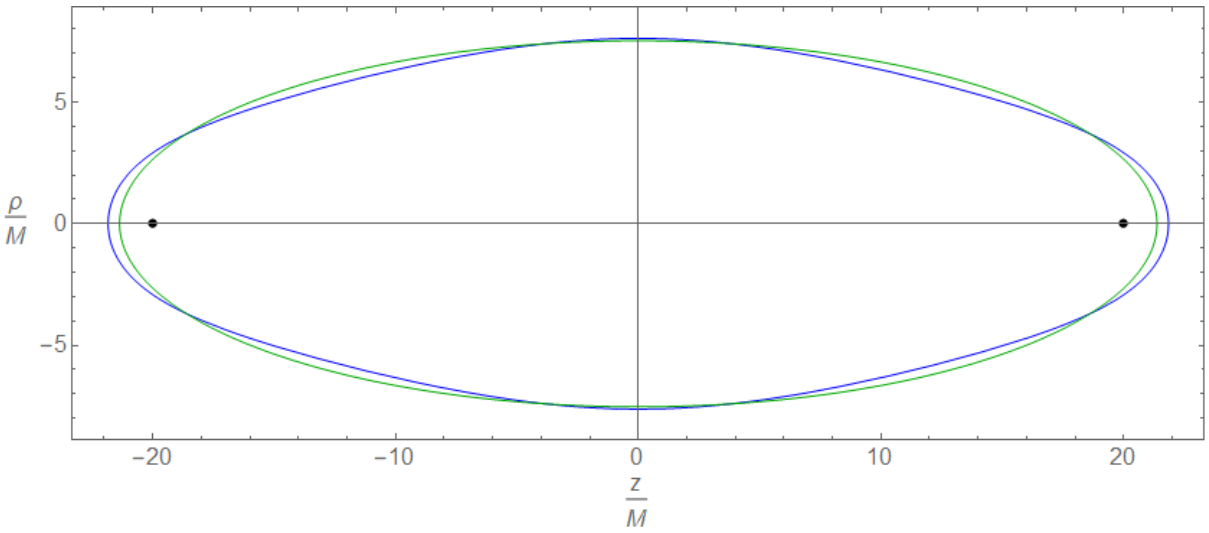

Figure 17: A direct comparison between the outer orbit in the cylinder case (blue) and ellipse C (green). The latter is an approximation of the former. The focal points of the ellipse coincide with the coordinates of the black holes, which are shown as black dots.

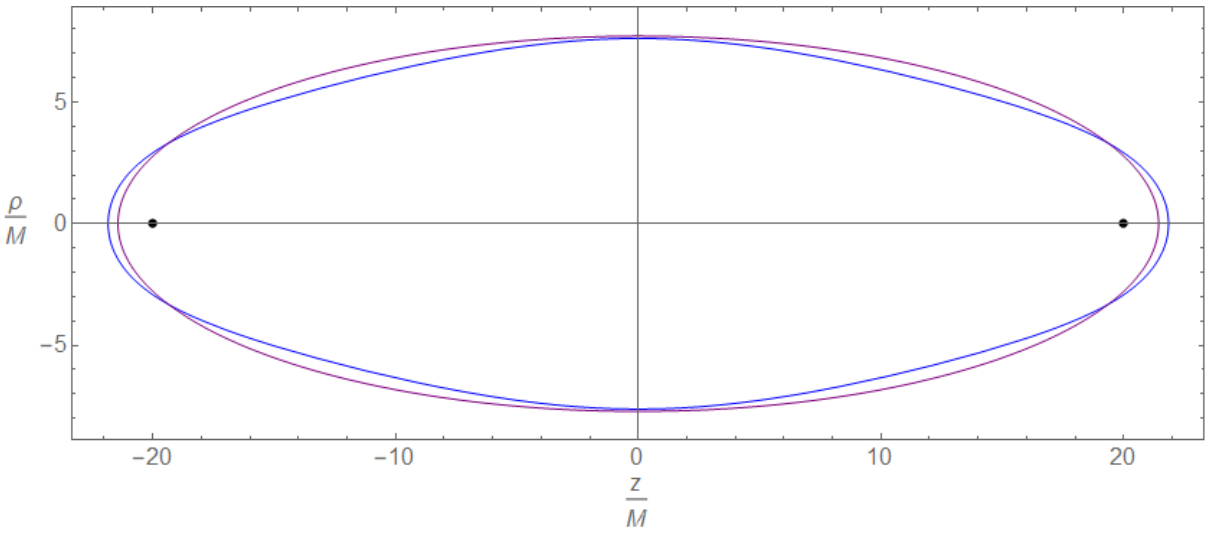

Figure 18: A direct comparison between the outer orbit in the cylinder case (blue) and ellipse D (purple). The latter is an approximation of the former, where we have chosen to have equal areas. Moreover, the focal points of the ellipse coincide with the coordinates of the black holes, which are shown as black dots.

4.2 Triangular case

We will now take a look at another configuration of a three black hole spacetime, where we have placed the three black holes in a triangle. All black holes have equal mass M and are separated by $a = 20M$. We will call this scenario the triangular case. In this scenario, we do not have axial symmetry anymore. Consequently, the angular momentum L is no longer conserved. Therefore it is more convenient to work in Cartesian coordinates. The metric then has the following form:

$$ds^2 = -\frac{dt^2}{U^2} + U^2(dx^2 + dy^2 + dz^2), \tag{4.2.1}$$

with

$$U = 1 + \frac{M}{\sqrt{\left(x + \frac{\sqrt{3}}{6}a\right)^2 + y^2 + \left(z - \frac{1}{2}a\right)^2}} \tag{4.2.2}$$

$$+\frac{M}{\sqrt{\left(x - \frac{\sqrt{3}}{3}a\right)^2 + y^2 + z^2}} + \frac{M}{\sqrt{\left(x + \frac{\sqrt{3}}{6}a\right)^2 + y^2 + \left(z + \frac{1}{2}a\right)^2}}.$$

The Lagrangian is now given by

$$\mathcal{L} = \frac{1}{2}\left(-\frac{\dot{t}^2}{U^2} + U^2(\dot{x}^2 + \dot{y}^2 + \dot{z}^2)\right) = -\frac{1}{2}\epsilon. \tag{4.2.3}$$

In a similar way as discussed in section 2.5, we can now determine the equations of motion. Since there is no conservation of angular momentum, we have an extra equation compared to the cylindrical case. Our system of equations of motion is then given by:

$$\dot{t} = EU^2 \tag{4.2.4a}$$

$$\dot{x} = \frac{p_x}{U^2} \tag{4.2.4b}$$

$$\dot{p}_x = \frac{1}{U^3}\left(E^2U^4 + p_x^2 + p_y^2 + p_z^2\right)\frac{\partial U}{\partial x} \tag{4.2.4c}$$

$$\dot{y} = \frac{p_y}{U^2} \tag{4.2.4d}$$

$$\dot{p}_y = \frac{1}{U^3}\left(E^2U^4 + p_x^2 + p_y^2 + p_z^2\right)\frac{\partial U}{\partial y} \tag{4.2.4e}$$

$$\dot{z} = \frac{p_z}{U^2} \tag{4.2.4f}$$

$$\dot{p}_z = \frac{1}{U^3}\left(E^2U^4 + p_x^2 + p_y^2 + p_z^2\right)\frac{\partial U}{\partial z}. \tag{4.2.4g}$$

Despite the absence of axial symmetry, this spacetime does have reflection symmetry. There are three such symmetry axes. These axes arise when one extends the lines between the black hole coordinates and the origin. This means that when we have found a closed photon orbit which is symmetric in one of these three axes, there are another two orbits which have the same shape and are symmetric in the other two axes.

Figure 19 shows all closed photon orbits which are symmetric in the x-axis. The same types of orbits are present for the other two symmetry axes, but for clarity these orbits are not included in Figure 19, with the exception of the red orbits.

The red orbits are by approximation circular. The outer blue orbit now has a shape similar to a triangle with round edges. We also see that the outer orbit (purple) and the 8-shaped orbit (green) from the two black hole meridian plane are present. All orbits which are symmetric in the x-axis have initial positions x_0 as stated in Table 3, $y_0 = 0$ and $z_0 = 0$. Their initial momenta are given by $p_{x_0} = 0$, $p_{y_0} = 0$ and $p_{z_0} = EU_0^2$. We have chosen $E = 1$ and U_0 can be determined by substituting the initial coordinates into Eq. (4.2.2). The green orbit is defined in a tricky way, since we chose to only have initial momentum in the z-direction. It initiates above the uppermost black hole, after which it will encircle the other two black holes.

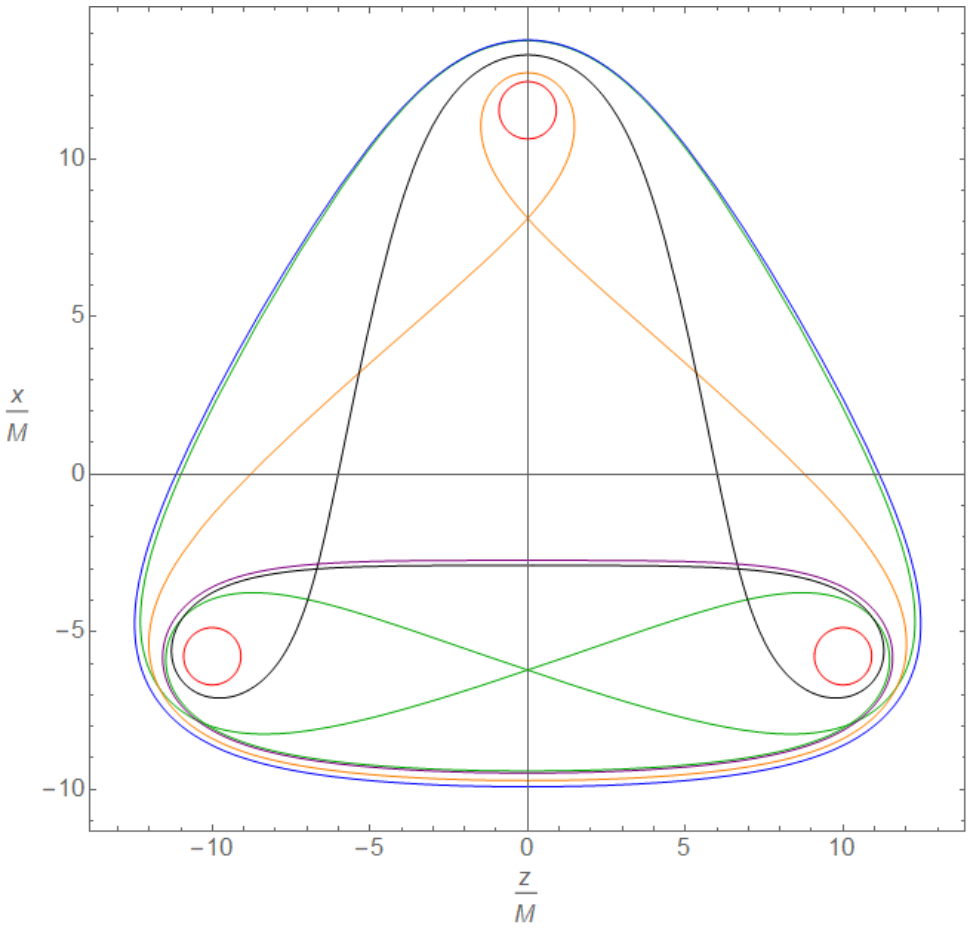

Figure 19: All closed photon orbits in the triangle case which are symmetric in the x-axis, along with the two lower circular orbits which are symmetric in the other two axes yielding reflection symmetry. These axes can be obtained by rotating the x-axis 120 and 240 degrees. The three black holes are separated by a distance $a = 20M$.

Orbit(s)	x_0/M	λ_{max}	T/M
Blue	13.776123097	76.6671	137.587
Green	13.759404603	127.3990	244.463
Black	13.305243408	77.7539	163.214
Orange	12.740009968	76.4870	152.192
Red (top)	12.459135065	5.7108	27.647
Purple	−2.732826144	52.1999	103.226

Table 3: The initial coordinates x_0, the values of the affine parameter for one orbit λ_{max} and the orbital periods T of the orbits symmetric in the x-axis from Figure 19.

5 Comparing two and three black hole spacetimes

In this chapter we will compare two and three black hole spacetimes. In particular, we will compare a spacetime in which one black hole is two times more massive than the other with a spacetime in which the separation between three black holes is varied.

5.1 Two black holes with different mass

We start by looking at a binary system where one black hole has twice the mass of the other black hole. We choose a cylindrical coordinate system and look at the meridian plane only. The mass difference is embedded in the functional form of U. If we place both black holes symmetrically at the z-axis at $z = \pm a$ and we choose the black hole on the right to have the bigger mass, U is defined as:

$$U = 1 + \frac{2M}{\sqrt{\rho^2 + (z-a)^2}} + \frac{M}{\sqrt{\rho^2 + (z+a)^2}}. \tag{5.1.1}$$

Figure 20 shows a contour plot of the Kretschmann scalar for this binary system, characterized by $a = 10M$. We observe that the spacetime is more strongly curved near the more massive black hole.

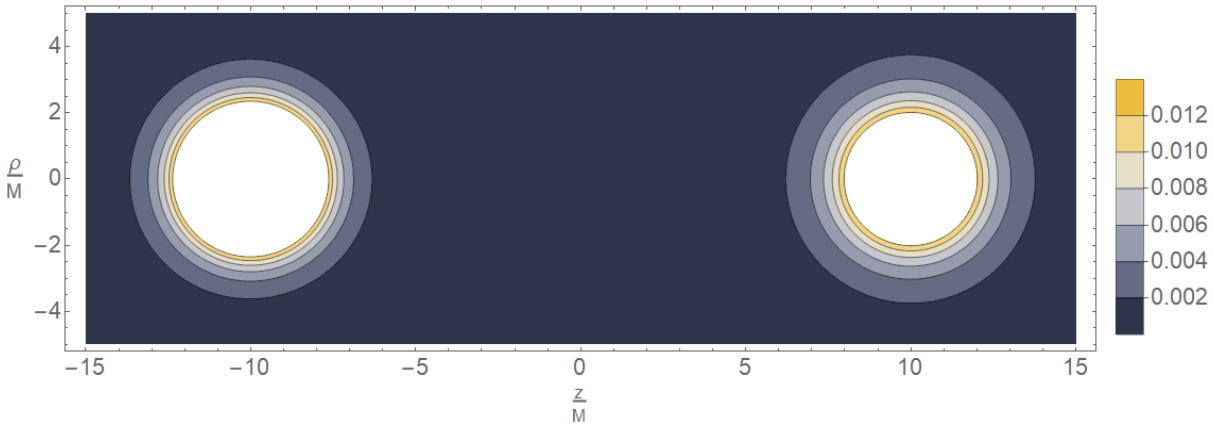

Figure 20: A contour plot of the Kretschmann scalar in the two black hole meridian plane with mass difference, characterized by $a = 10M$.

Figure 21 shows all closed photon orbits around this binary system with $a = 10M$. The same kind of orbits are present as in the case where both black holes have equal mass. Since the black hole on the right has twice the mass of the black holes on the left, the gravitational pull on the photon is stronger near the more massive black hole. Therefore the photon needs to maintain a larger distance to the black hole on the right in order to stay in its orbit.

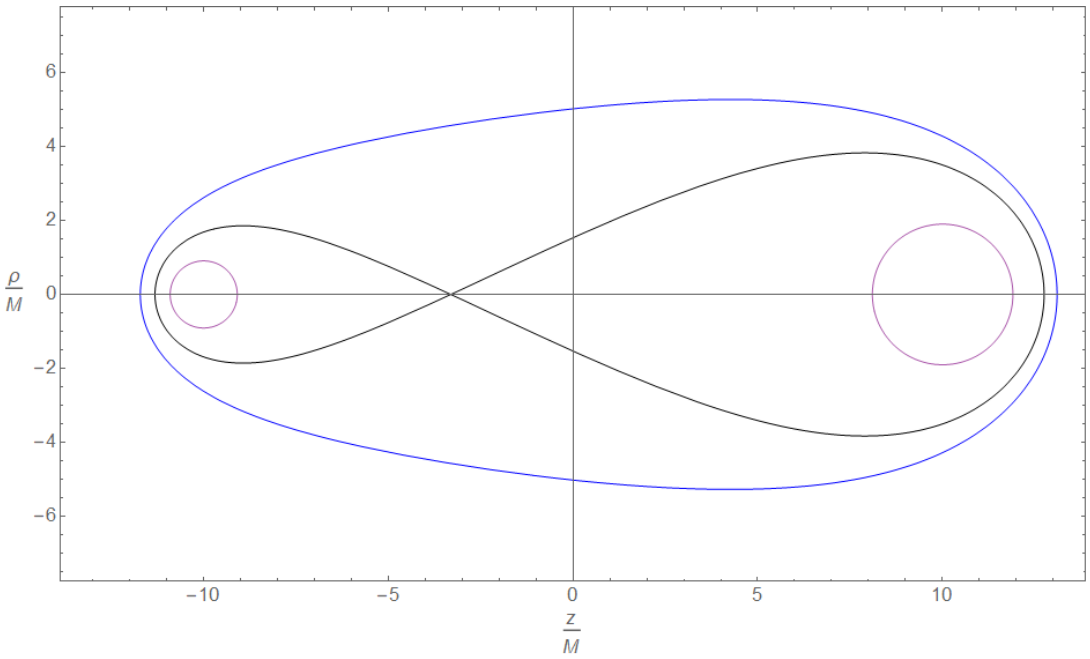

Figure 21: All closed photon orbits around a binary in the meridian plane with the black hole on the right having twice the mass of the black hole on the left. The plane is characterized by a separation constant of $a = 10M$.

Table 4 shows the initial coordinates on the z-axis, the values of λ_{max} and the orbital periods T of all orbits from Figure 21. The initial coordinate on the ρ-axis is given by $\rho_0 = 0$ for all orbits. The initial momenta are given by $(p_{\rho_0}, p_{z_0}) = (EU_0^2, 0)$, where U_0 can be obtained by substituting z_0 and ρ_0 into Eq. (5.1.1). The energy is kept constant at a value of $E = 1$. The values of T are obtained by numerically integrating Eq. (3.1.1).

Orbit	z_0/M	λ_{max}	T/M
Blue	13.107806400	58.7470	119.372
Black	12.756541134	56.3660	125.784
Purple (right)	11.912191020	11.9620	52.784
Purple (left)	−10.912609185	5.7109	27.647

Table 4: The initial coordinates z_0, the values of the affine parameter for one orbit λ_{max} and the orbital periods T of the orbits from Figure 21.

We use Taylor expansions again to determine the radius $r = \sqrt{\rho^2 + (z \pm a)^2}$ of the (roughly) circular orbits from Figure 21, which are shown in purple. From a first order expansion in a/M we obtain the following value of r for the circular orbit on the left:

$$\frac{r}{M} \simeq 1 - \frac{M}{a}. \tag{5.1.2}$$

This radius is slightly smaller than the approximated radii of the circular orbits from Figure 3, given by Eq. (3.1.2), where both black holes have equal mass. Since

we now have a more massive black hole present, the gravitational pull from that black hole felt by the photon needs to be compensated by maintaining a smaller distance to the left black hole. Substituting $a = 10M$ in Eq. (5.1.2) results in an approximated value of $r \simeq 0.9M$, which slightly underestimates the numerical value of $r = 0.9126M$.

In a similar way we can find an approximated value of the radius of the circular orbit on the right. We obtain the following relation:

$$\frac{r}{M} \simeq 2 - \frac{M}{a}. \tag{5.1.3}$$

Substituting $a = 10M$ gives us a radius of $r \simeq 1.9M$, which slightly underestimates the numerical value of $r = 1.9122M$.

5.2 Three black holes with different separation

We will now investigate a three black hole spacetime where all black holes have equal mass, but the distance between them varies. We will again take a cylindrical coordinate system and restrict ourselves to the meridian plane. We will place the black holes on the z-axis at $z = -a$, $z = a - \delta$ and $z = a + \delta$. This gives rise to the following form of U:

$$U = 1 + \frac{M}{\sqrt{\rho^2 + (z+a)^2}} + \frac{M}{\sqrt{\rho^2 + (z-(a-\delta))^2}} + \frac{M}{\sqrt{\rho^2 + (z-(a+\delta))^2}}. \tag{5.2.1}$$

We have chosen this configuration of the three black holes, because this allows us to look at a spacetime where the middle and right black hole are placed close together while the black hole on the left is at a larger distance. This means we will restrict ourselves to a scenario in which $\delta \ll a$. If we take the limit $\delta \to 0$ in Eq. (5.2.1), we observe that we get the same functional form of U as given in Eq. (5.1.1). Hence, by choosing a small value of δ we are able to compare a three black hole meridian plane with a two black hole meridian plane.

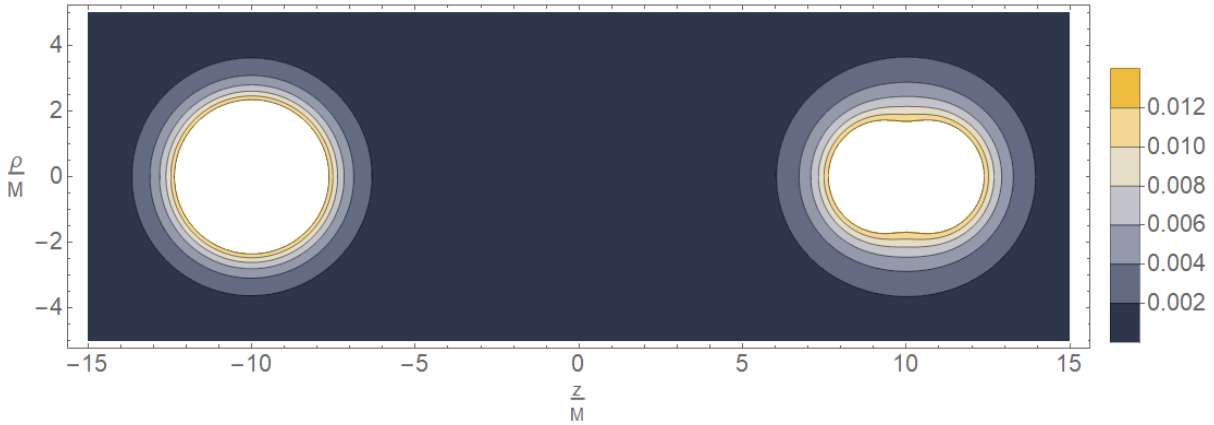

Figure 22: A contour plot of the Kretschmann scalar in the three black hole meridian plane, characterized by U as given in Eq. (5.2.1) with $a = 10M$ and $\delta = 0.5M$.

Figure 22 shows the contour plot of the Kretschmann scalar of the three black hole meridian plane, characterized by U as given in Eq. (5.2.1) with $a = 10M$ and $\delta = 0.5M$. Figure 23 shows the closed photon orbits in this spacetime. The initial coordinates of all orbits are given by $\rho_0 = 0$ and z_0 as stated in Table 5. The initial momenta are given by $(p_{\rho_0}, p_{z_0}) = (EU_0^2, 0)$, where $E = 1$ and U_0 can be obtained by substituting z_0 and ρ_0 into Eq. (5.2.1). Table 5 also gives the values of λ_{max} and the orbital period T of each orbit. The orbital period is determined by numerical integration of Eq. (3.1.1) with U as given in Eq. (5.2.1).

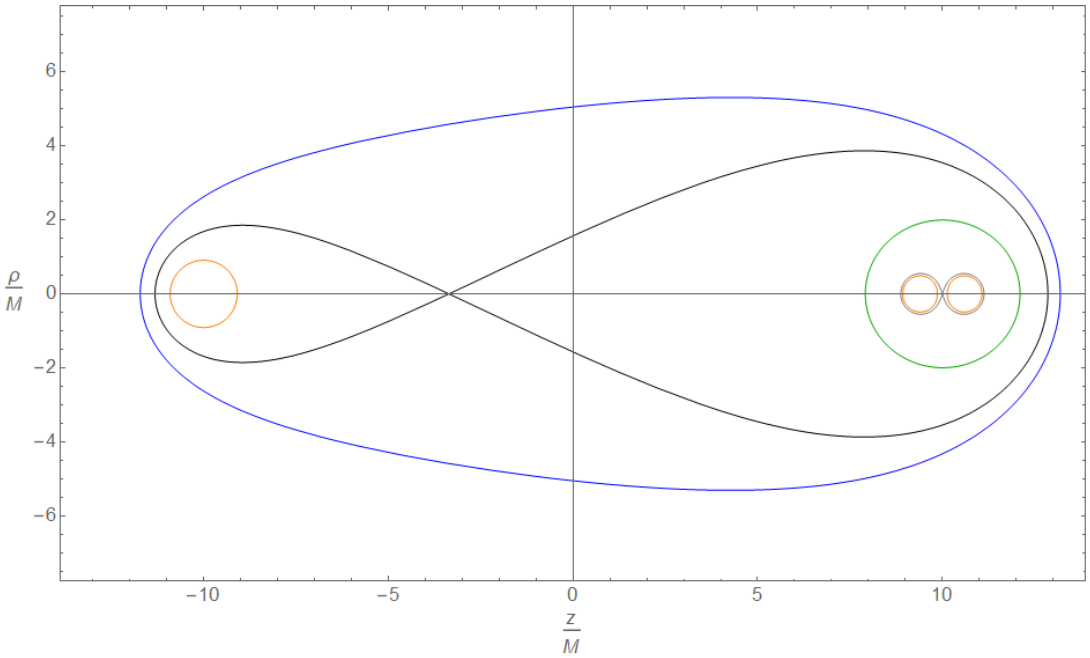

Figure 23: Closed photon orbits in a three black hole meridian plane, characterized by U as given in Eq. (5.2.1) with $a = 10M$ and $\delta = 0.5M$.

Orbit	z_0/M	λ_{max}	T/M
Blue	13.194522680	58.9394	119.513
Black	12.858206565	56.5864	125.983
Green	12.105141410	12.8605	53.620
Grey	11.129727498	6.9126	106.706
Orange (right)	11.075016612	3.0241	52.199
Orange (middle)	9.867518581	3.0169	52.268
Orange (left)	−10.912563078	5.7105	27.649

Table 5: The initial coordinates z_0, the values of the affine parameter for one orbit λ_{max} and the orbital periods T of the orbits from Figure 23.

We observe that Figure 23 bears a lot of resemblance with Figure 21. The radius $r = \sqrt{\rho^2 + (z+a)^2}$ of the left circular orbit from Figure 23 can again be approximated using a Taylor expansion for $a \gg M$. As a result we obtain the same relation for r as found for the left circular orbit from Figure 21, given by Eq. (5.1.2).

Since the distance between the middle and right black hole is relatively small, the green orbit from Figure 23 can be approximated by a circle as well. We Taylor expand for $\delta \ll a$ and $a \gg M$ and find the same relation as given in Eq. (5.1.3) for the radius $r = \sqrt{\rho^2 + (z-a)^2}$ of the green orbit. We can conclude that the size of the green orbit from Figure 23 is approximately equal to the size of the right purple orbit from Figure 21. However, the green orbit is expected to be a little bit larger than the purple orbit, since we choose $\delta > 0$. The radii of both orbits only coincide when $\delta = 0$.

Figure 24 shows a zoomed-in version of Figure 23, focused on the middle and right black hole. The orbits which each enclose one black hole are shown in orange. We notice that these orbits are not perfectly circular; they are somewhat squeezed. For clarity, the coordinates of the black holes are given as black dots in Figure 24. Also note that the black holes do not coincide with the centre of the orange orbits. Hence, the orbits are not only squeezed but also somewhat shifted towards the outside.

The physical reason is that both black holes are placed very close together. Therefore, the gravitational field from one black hole differs significantly at every point of the orbit around the other black hole. Hence, a photon orbiting one black hole experiences a relatively large gravitational pull from the other black hole in addition to the gravitational pull from the black hole it is orbiting. When the distance to the other black hole becomes too small, the photon needs to maintain an even closer distance to the black hole it is encircling.

Figure 24 also shows two dashed circles around each black hole. These are not actual orbits, but are circles showing how a circular orbit would look. The centre of all four circles coincide with the coordinates of the black holes. The diameters of the blue circles are equal to the horizontal diameters of the orange orbits, while the diameters of the purple circles are equal to the vertical diameters of the orange orbits. Since the orbits are squeezed, the purple circles are bigger than the blue circles.

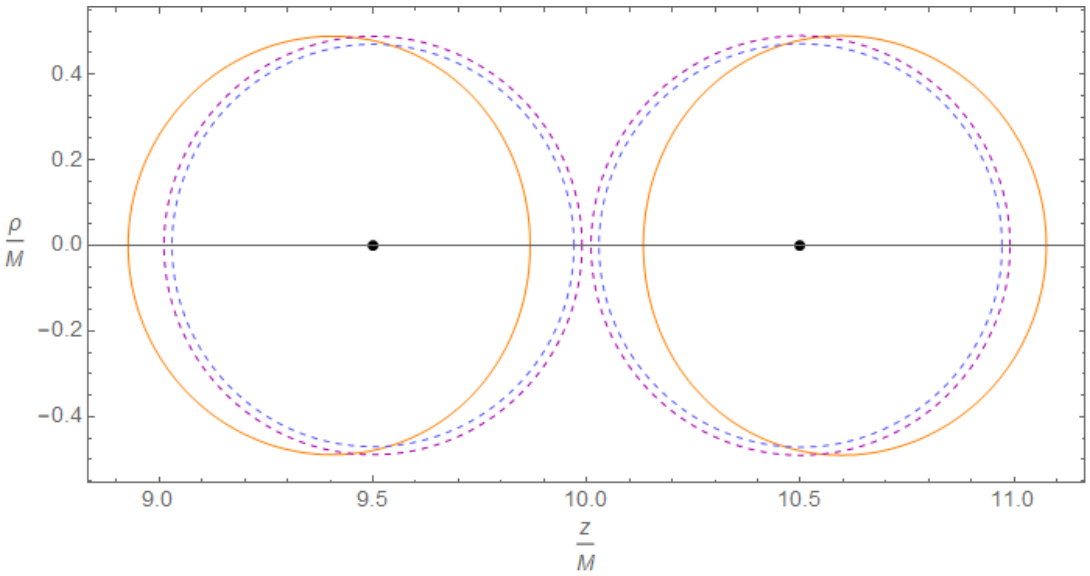

Figure 24: A direct comparison between the two smallest orbits from Figure 23 (orange) and four dashed circles which emphasise how perfectly circular orbits would look. The diameters of the blue circles are equal to the horizontal diameter of the orange orbits and are given by $d_L = 0.9403M$ and $d_R = 0.9427M$ for the left and right blue circle, respectively. The diameters of the left and right purple circles are given by $d_L = 0.9779M$ and $d_R = 0.9801M$, respectively, and are equal to the vertical diameter of the orange orbits.

5.3 Smiley plots

The diameters of the middle and right orange orbits from Figure 23 are not equal, because of the presence of the most left black hole. In this section, we will study how this black hole affects the size of the orbits around the middle and right black hole. Figure 25 is a zoomed in version of Figure 23 and shows the green, grey and smallest orange orbits from this plane. The black dots represent the coordinates of the middle and right black hole. The large purple orbit from Figure 21 is also shown. Its radius is somewhat smaller than the radius of the green orbit, as expected. Since the plot from Figure 25 resembles a smiley, we will refer to such plots as smiley plots.

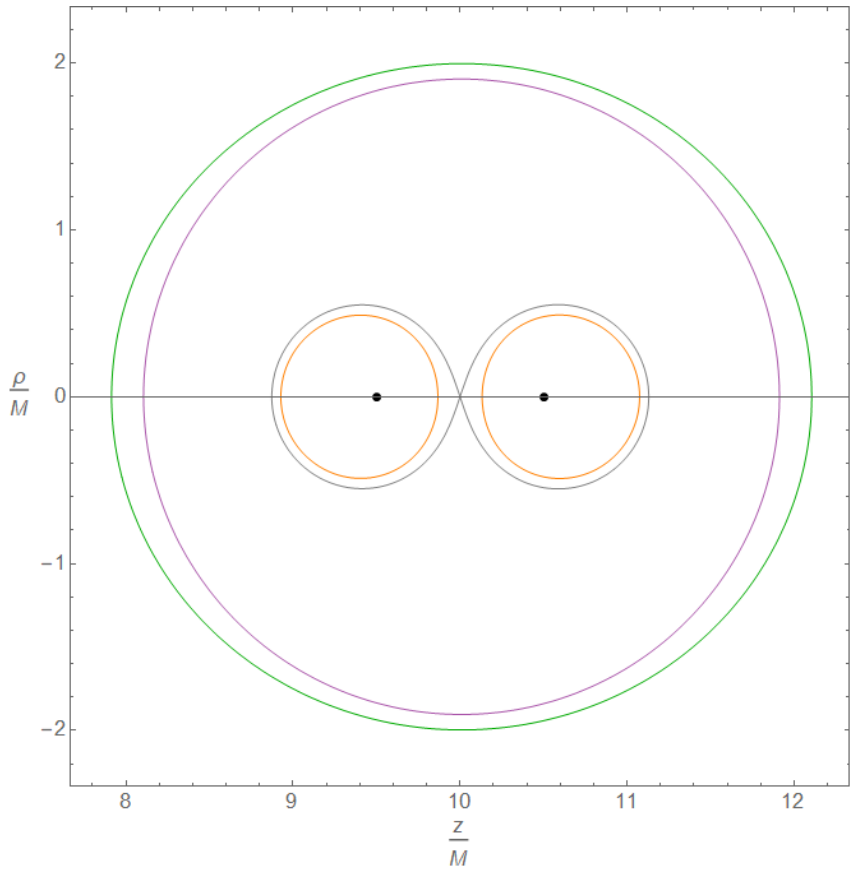

Figure 25: A direct comparison between the large purple orbit from the two black hole scenario (Figure 21) and the green orbit from the three black hole scenario (Figure 23). The grey and smallest orange orbits from Figure 23 are shown as well. The black dots correspond to the coordinates of the middle and right black hole from the three black hole meridian plane with separation difference.

For a more direct comparison, we will now also have a look at a two black hole meridian plane with a small separation constant:

$$U = 1 + \frac{M}{\sqrt{\rho^2 + (z - (a - \delta))^2}} + \frac{M}{\sqrt{\rho^2 + (z - (a + \delta))^2}}. \tag{5.3.1}$$

The distance between both black holes is now given by 2δ. In order to compare this case with the three black hole case with separation difference, we choose values of $a = 10M$ and $\delta = 0.5M$. All orbits are shown in Figure 26. The black dots represent the coordinates of both black holes. All orbits have initial coordinates $\rho_0 = 0$ and z_0 as given in Table 6. This table also gives the values of λ_{max} and the orbital period T for each orbit. The orbital period is determined by numerically integrating Eq. (3.1.1). The initial momenta of all orbits are given by $(p_{\rho_0}, p_{z_0}) = (EU_0^2, 0)$ with $E = 1$ and U_0 obtained by substituting ρ_0 and z_0 into Eq. (5.3.1).

Figure 27 is a plot of all orbits from Figure 25 and Figure 26. Figure 28 is a zoomed-in version, focused on the smallest orbits. From both figures we can conclude that the presence of an extra black hole reduces the size of the orbits which do not encircle this extra black hole. After all, the green, grey and orange orbits are smaller than the blue, black and red orbits, respectively. This effect is less significant if the extra black hole is placed at an even larger distance.

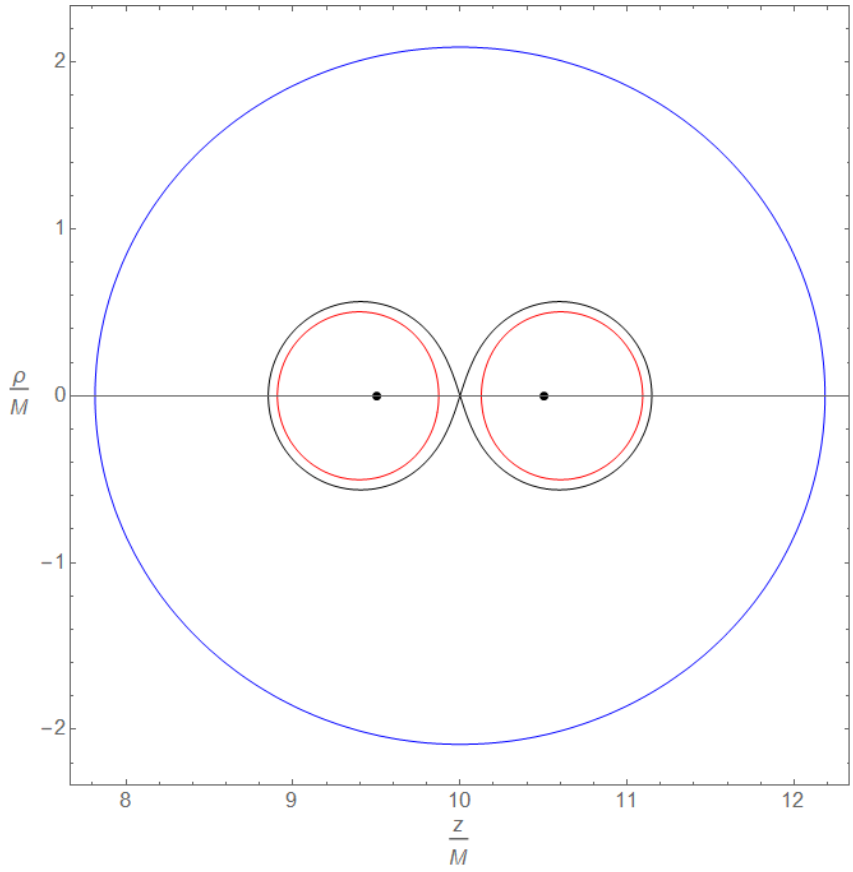

Figure 26: All closed photon orbits in a two black hole meridian plane, characterized by U as given in Eq. (5.3.1) with $a = 10M$ and $\delta = 0.5M$. The black dots correspond to the black hole coordinates.

Orbit	z_0/M	λ_{max}	T/M
Blue	12.185091108	13.4321	50.991
Black	11.147991968	7.0560	104.027
Red (right)	11.093440039	3.1016	50.991
Red (left)	8.906559961	3.1016	50.991

Table 6: The initial coordinates z_0, the values of the affine parameter for one orbit λ_{max} and the orbital periods T of the orbits from Figure 26.

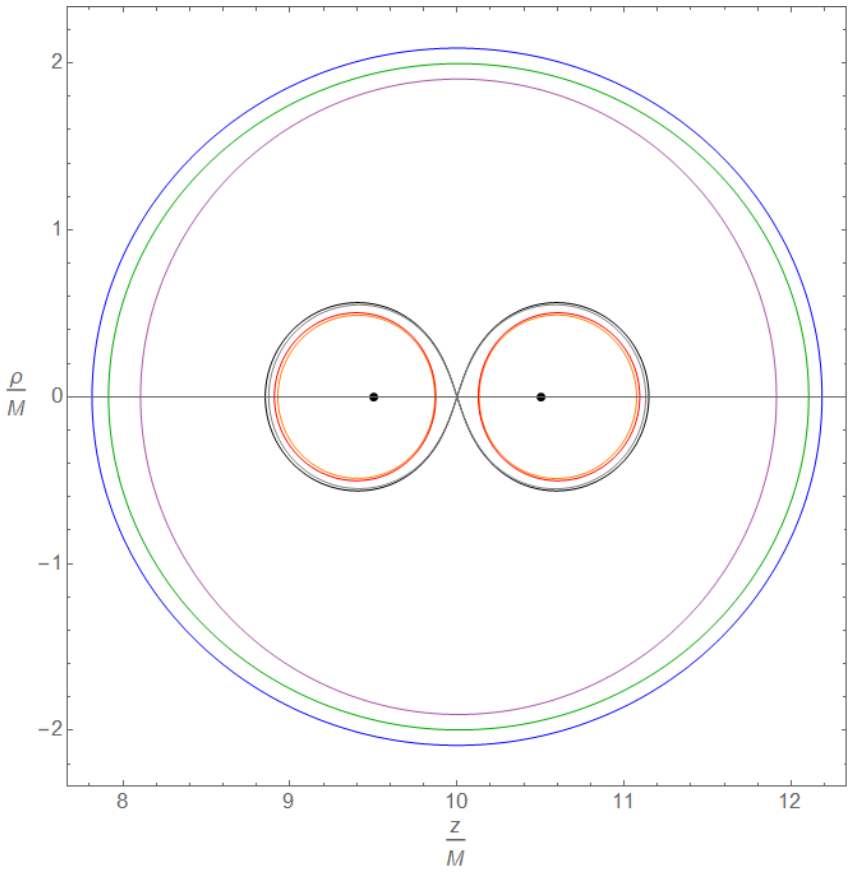

Figure 27: A direct comparison between all orbits from Figure 25 and Figure 26.

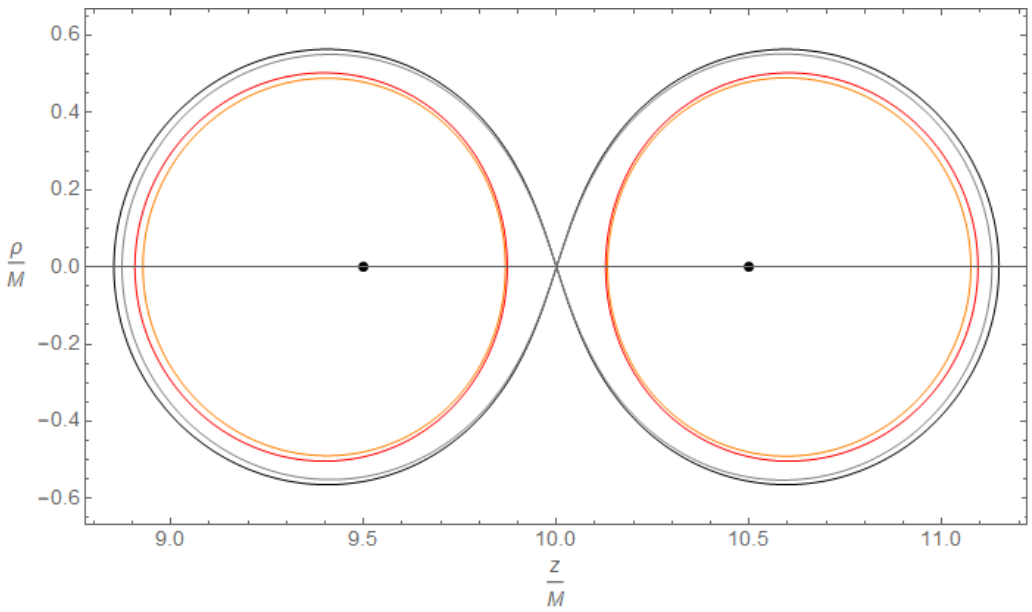

Figure 28: A zoomed-in version of Figure 27.

6 Conclusion and Discussion

The work in this thesis provides a toy model for studying the motion of photons around multiple black holes. We started by looking at a relatively simple single black hole solution, which is the Schwarzschild solution. After discussing null geodesics around the Schwarzschild black hole, we advanced to the Reissner-Nordström black hole. This solution is an extension of the Schwarzschild solution since it allows the black hole to have an electric charge. By only looking at the extremal case, where the mass and the charge of the black hole are equivalent, and by performing a coordinate transformation, we advanced to the Majumdar-Papapetrou solution. This allowed us to look at multiple black hole spacetimes, where we were able to give each individual black hole a mass (and an equivalent charge) M_j and place it at a coordinate $\mathbf{r}_j$.

The next step was to determine a set of equations of motion. Two equations of motion were determined by using Killing vectors, while the rest were determined by using a hybrid Lagrangian/Hamiltonian approach.

In chapter three, we looked at a MP spacetime with two black holes. We first looked at the meridian plane, which allowed angular momentum for the photons circling these black holes. There are three types of closed photon orbits in this plane: (roughly) circular orbits, an orbit enclosing both horizons and and 8-shaped orbit. By using Taylor expansions, expressions for the radius and the orbital period were found for both circular orbits. The orbital periods of the outer orbit and the 8-shaped orbit were approximated by parametrizing the shape of both orbits. Secondly, we looked at the $z = 0$ plane. Various orbits were found, including two circular orbits. After a stability analysis we could conclude that the outer circular orbit is unstable and that more massive black holes yield more stable orbits. There is no evident connection between the photon orbits in the meridian plane and the $z = 0$ plane, since both planes are perpendicular to each other.

In chapter four, we looked at three black hole MP spacetimes. At first we looked at the cylindrical case where all three black holes were placed on the z-axis with a constant separation. Various photon orbits were found, including the orbits which were present in the two black hole meridian plane. By using Taylor approximations we could conclude that the radius of the middle circular orbit is smaller than the radii of the left and right circular orbits. After a stability analysis we also found that the left and right circular orbits are more stable than the middle circular orbit. The outer orbit was best approximated by an ellipse. Secondly, we looked at a triangular configuration of the three black holes. Since we did not have axial symmetry anymore, angular momentum was allowed for the photons. Therefore, we needed to define an extra equation for the evolution of the angular coordinate ϕ. We used the threefold reflection symmetry in this plane to find many photon orbits.

We compared two and three black hole MP spacetimes in chapter 5. At first we varied the mass in the two black hole spacetime and varied the separation in the

three black hole case. We were able to conclude that the corresponding orbits in both spacetimes will have the same size when two black holes in the three black hole spacetime are placed at the same position. We did an analysis regarding the effect of an extra black hole. Second, we compared a two black hole spacetime with small separation and a three black hole spacetime where one black hole was placed at a relatively large distance from two closely placed black holes. We found that the placement of an extra black hole reduces the size of the photon orbits around the binary.

In this thesis we only looked at two and three black hole MP spacetimes. We chose not to look at spacetimes with more than three black holes, since all the techniques we used would be equivalent for these spacetimes. Hence, we thought that it would be more interesting to study the properties of all orbits we found in the two and three black hole spacetimes in more detail.

One of the properties we discussed is the stability of orbits. In general, the orbits in all meridian planes are unstable. The initial conditions of these orbits had to be given very precisely so that a photon could complete one closed orbit. We found that the Lyapunov exponent is proportional to $1/M$ for circular orbits in this plane. Hence, more massive black holes yield more stable circular photon orbits. In the $z = 0$ plane, we found one stable and one unstable circular orbit. The Lyapunov exponent of the unstable circular orbit exhibits the same behaviour as in the meridian planes.

The instability of most orbits is closely related to some phenomena which have not been discussed in this thesis. One of these phenomena is chaotic scattering [3]. In all meridian planes, it is not possible to predict whether null geodesics that initiate at infinity will escape towards infinity or fall into one of the black holes [13]. Another aspect related to the instability of orbits are the quasinormal modes of the black holes [4]. Since the extension to multiple black hole makes it quite difficult to do an elaborated analysis in both phenomena, they were not discussed in further detail in this thesis.

The approach we used in this thesis is purely theoretical, since we made some assumptions. At first we chose to work with static spacetimes, which are irrotational. Solutions which allow objects to rotate are the Kerr and Kerr-Newman solutions. However, a multiple black hole solution such as the Majumdar-Papapetrou solution is quantitatively and qualitatively different from these solutions. Therefore they are not useful for our research. Secondly, the black holes in all MP spacetimes are maximally charged Reissner-Nordström black holes. The extremal Reissner-Nordström black hole is very unstable. If the mass of the black hole slightly increases, the situation will fall back into the case where the mass is greater than the charge [5]. Also, since there has not been an observation of a charged black hole to date, it is difficult to compare the results in this thesis with real life observations such as the black hole picture. Nevertheless, the framework provided in this thesis is a nice toy model for photon paths around multiple black holes.

References

[1] Black Hole Perturbation Toolkit. (bhptoolkit.org).

[2] Astronomers Capture First Image of a Black Hole. (https://eventhorizontelescope.org/press-release-april-10-2019-astronomers-capture-first-image-black-hole), 2019.

[3] J. M. Aguirregabiria. Chaotic scattering around black holes. *Phys. Lett. A*, 224:234–238, 1997.

[4] T. Assumpcao, V. Cardoso, A. Ishibashi, M. Richartz, and M. Zilhao. Black hole binaries: ergoregions, photon surfaces, wave scattering, and quasinormal modes. *Phys. Rev. D*, 98(6):064036, 2018.

[5] S. M. Carroll. Lecture notes on general relativity. 12 1997.

[6] S. Chandrasekhar. The Two Center Problem in General Relativity: The Scattering of Radiation by Two Extreme {Reissner-Nordstrom} Black Holes. *Proc. Roy. Soc. Lond. A*, 421:227–258, 1989.

[7] N. J. Cornish and J. J. Levin. Lyapunov timescales and black hole binaries. *Class. Quant. Grav.*, 20:1649–1660, 2003.

[8] L. E. Dickson. *First course in the theory of equations.* John Wiley and sons, New York, 1922.

[9] I. Gkigkitzis, I. Haranas, and O. Ragos. Kretschmann Invariant and Relations Between Spacetime Singularities, Entropy and Information. *Physics International*, 5(1):103–111, 2014.

[10] M. Patil, P. Mishra, and D. Narasimha. Curious case of gravitational lensing by binary black holes: a tale of two photon spheres, new relativistic images and caustics. *Phys. Rev. D*, 95(2):024026, 2017.

[11] M. Rood. Black hole shadows - Shining light on black holes and their mimickers. 2020.

[12] J. Shipley and S. R. Dolan. Binary black hole shadows, chaotic scattering and the Cantor set. *Class. Quant. Grav.*, 33(17):175001, 2016.

[13] U. Yurtsever. Geometry of chaos in the two center problem in general relativity. *Phys. Rev. D*, 52:3176–3183, 1995.

A Circular orbits

In this section we will derive the relations for the radius $r = \sqrt{\rho^2 + z^2}$ and the orbital period T of circular orbits in terms of the separation constant a. We will do this once for the middle circular orbit in the three black hole meridian plane. At the end of these derivations we will note how these relations can be derived for the other orbits.

A.1 Approximation of the radius

We will start with the condition of a circular orbit. For the middle circular orbit in the three black hole meridian plane we have:

$$r^2 = \rho^2 + z^2. \tag{A.1.1}$$

In this equation r is the radius of the circular orbit. Therefore it is constant. Differentiating this condition with respect to the affine parameter λ gives us:

$$\rho\dot{\rho} + z\dot{z} = 0. \tag{A.1.2}$$

Substituting Eq. (2.5.21c) and Eq. (2.5.21e) in this relation gives us:

$$p_\rho \rho + p_z z = 0. \tag{A.1.3}$$

We can differentiate this equation again with respect to λ. This leads to:

$$\dot{p}_\rho \rho + \dot{p}_z z + p_\rho \dot{\rho} + p_z \dot{z} = 0. \tag{A.1.4}$$

After substituting Eq. (2.5.21c) and Eq. (2.5.21e) we obtain:

$$\dot{p}_\rho \rho + \dot{p}_z z + \frac{p_\rho^2}{U^2} + \frac{p_z^2}{U^2} = 0. \tag{A.1.5}$$

Now we use the energy relation from Eq. (2.5.12). Since the angular momentum is zero in the meridian plane, the effective potential is equal to 0. Substituting Eq. (2.5.21c) and Eq. (2.5.21e) results in the following relation:

$$p_\rho^2 + p_z^2 = E^2 U^4. \tag{A.1.6}$$

This relation can be substituted in Eq. (2.5.21d) and Eq. (2.5.21f). As a result we obtain

$$\dot{p}_\rho = 2E^2 U \frac{\partial U}{\partial \rho} = E^2 \frac{\partial}{\partial \rho}(U^2) \tag{A.1.7}$$

for the ρ-momentum derivative, since $L = 0$. For the z-momentum derivative we get:

$$\dot{p}_z = 2E^2 U \frac{\partial U}{\partial z} = E^2 \frac{\partial}{\partial z}(U^2). \tag{A.1.8}$$

Now we will substitute Eq. (A.1.6), Eq. (A.1.7) and Eq. (A.1.8) into Eq. (A.1.5). This gives us a suitable condition for circular orbits to work with, which we will call the circular orbit equation:

$$\Big(\rho\frac{\partial}{\partial\rho}+z\frac{\partial}{\partial z}\Big)U^2+U^2=0. \tag{A.1.9}$$

Since this relation only depends on ρ and z and no longer on the momenta, we can start using Taylor approximations. At first we look at U as given in Eq. (4.1.1). A first order Taylor expansion for $a \gg M$ gives us:

$$U \simeq 1+\frac{M}{\sqrt{\rho^2+z^2}}+\frac{2M}{a}. \tag{A.1.10}$$

Now we expand the circular orbit equation (A.1.9) to the first order for $a \gg M$. After simplifying we find:

$$\left(1+\frac{M}{\sqrt{\rho^2+z^2}}\right)\left(1-\frac{M}{\sqrt{\rho^2+z^2}}\right)+\frac{4M}{a}\simeq 0. \tag{A.1.11}$$

We can now substitute Eq. (A.1.1) and solve for the radius r. We obtain:

$$\frac{r}{M}\simeq\Big(1+\frac{4M}{a}\Big)^{-\frac{1}{2}}. \tag{A.1.12}$$

We can Taylor expand this again to the first order for $a \gg M$. This gives us the relation for r for large separations:

$$\frac{r}{M}\simeq 1-\frac{2M}{a}. \tag{A.1.13}$$

The approach is very similar for the other circular orbits in all meridian planes. Before starting with this derivation, you have to make a coordinate transformation such that the centre of your coordinate system coincides with the centre of the circular orbit you are looking at. This will change your U as well. For example, if we make such a coordinate transformation in the two black hole meridian plane, we obtain the following value of U:

$$U=1+\frac{M}{\sqrt{\rho^2+z^2}}+\frac{M}{\sqrt{\rho^2+(z-2a)^2}}. \tag{A.1.14}$$

In this case we are looking at the left circular orbit from Figure 3. We can now repeat the same steps as before and arrive at the same circular orbit equation (A.1.9), only with different U. If we now repeat the steps of the Taylor expansions, we will reach a slightly different relation for r, which is:

$$\frac{r}{M}\simeq 1-\frac{M}{2a}. \tag{A.1.15}$$

A.2 Approximation of the orbital period

In order to find an approximation for the orbital period T we will first try to find an expression we can expand. Therefore we write $\rho = r\sin\alpha$ and $z = r\cos\alpha$. It is easy to show that

$$\dot{\rho}^2 + \dot{z}^2 = \dot{r}^2 + r^2\dot{\alpha}^2 = r^2\dot{\alpha}^2. \tag{A.2.1}$$

Since we assume that we are dealing with circular orbits, $\dot{r} = 0$. We now use the energy relation (2.5.12) with $L = 0$. This results in a relation for the energy E:

$$E = \sqrt{\dot{\rho}^2 + \dot{z}^2} = r\dot{\alpha}. \tag{A.2.2}$$

We take the positive sign here since we need the energy to be positive. We now substitute this relation into Eq. (3.1.1). This gives us:

$$T = E\int_0^{\lambda_{max}} U^2 d\lambda = \int_0^{\lambda_{max}} rU^2\dot{\alpha}d\lambda = \int_0^{2\pi} rU^2 d\alpha = 2\pi r U^2. \tag{A.2.3}$$

This equation is valid for all circular orbits. We can now substitute the expanded values of U and r, which we obtained from section A.1, into this equation. If we look at the middle circular orbit in the three black hole meridian plane for example, we will get the following equation for the orbital period:

$$\frac{T}{M} = 2\pi U^2\frac{r}{M} \simeq 2\pi\Big(1 + \frac{M}{(1-\frac{2M}{a})} + \frac{2M}{a}\Big)^2\Big(1 - \frac{2M}{a}\Big). \tag{A.2.4}$$

We can now do a final Taylor expansion to the first order for $a \gg M$. This will give us the approximated value of T for large separations:

$$\frac{T}{M} \simeq 8\pi\Big(1 + \frac{2M}{a}\Big). \tag{A.2.5}$$

B Lyapunov exponent

In this section we will derive an analytic expression for the Lyapunov exponent λ considering the unstable circular orbit in the two black hole $z = 0$ plane. In a similar way one can derive the Lyapunov exponent for the other circular orbits considered in this thesis. This will be discussed after the derivation of the $z = 0$ plane.

We will start by using the fact that λ is the eigenvalue of the linear stability matrix K_{ij}. The elements of this matrix are given by

$$K_{ij} = \left.\frac{\partial H_i}{\partial X_j}\right|_{X_i(t)} \tag{B.0.1}$$

where H_i is the Hamiltonian. The coordinates and momenta are given by $X_i(t)$. We will only consider the coordinates regarding the radial motion [7]. Therefore we have $X_i(t) = (r, p_r)$ for the two black hole $z = 0$ plane. The linear stability matrix then has the following form:

$$K_{ij} = \frac{1}{\dot{t}} \begin{pmatrix} \frac{\partial \dot{\rho}}{\partial \rho} & \frac{\partial \dot{\rho}}{\partial p_\rho} \\ \frac{\partial \dot{p}_\rho}{\partial \rho} & \frac{\partial \dot{p}_\rho}{\partial p_\rho} \end{pmatrix}. \tag{B.0.2}$$

The Lyapunov exponent is dependent on the time coordinate. Since time is relative, we divide each element of the stability matrix by $\dot{t}$. This leads to a time scale measured by an observer at infinity.

In the $z = 0$ plane we have ρ as our radial coordinate. Since we are looking at a circular orbit, ρ has a constant value. Therefore the diagonal elements of the stability matrix vanish. It is now given by

$$K_{ij} = \begin{pmatrix} 0 & K_1 \\ K_2 & 0 \end{pmatrix} \tag{B.0.3}$$

where

$$K_1 = \frac{1}{\dot{t}} \frac{\partial \dot{\rho}}{\partial p_\rho} = \frac{1}{\dot{t} U^2} \tag{B.0.4}$$

and

$$K_2 = \frac{1}{\dot{t}} \frac{\partial \dot{p}_\rho}{\partial \rho}. \tag{B.0.5}$$

Now we can easily obtain the eigenvalues of K_{ij} and an expression for λ:

$$\lambda = \sqrt{K_1 K_2}. \tag{B.0.6}$$

We would like to specify λ in terms of U. Therefore we have to find a suitable expression for K_2. That's why we first have a look at the energy relation from Eq. (2.5.12). Differentiating with respect to ρ yields

$$\dot{\rho} \frac{\partial \dot{\rho}}{\partial \rho} = -\frac{1}{2} V', \tag{B.0.7}$$

where V is the effective potential and $V' = \partial V/\partial\rho$. Using this relation, the energy relation and Eq. (2.5.21c) we can show that

$$\dot{p}_\rho = \frac{\partial \mathcal{L}}{\partial \rho} = \dot{\rho}\frac{\partial}{\partial \rho}\Big(U^2\rho\Big) = \frac{1}{2U^2}\frac{\partial}{\partial \rho}\Big(U^4\big(E^2 - V\big)\Big). \tag{B.0.8}$$

Now we will use the fact that we are dealing with a circular orbit. This means $\dot{\rho} = 0$. As a result we obtain $E^2 = V$ from Eq. (2.5.12) and $V' = 0$ from Eq. (B.0.7). Note that this does not imply that $V'' = 0$. We can now construct a suitable expression for K_2 by differentiating Eq. (B.0.8) with respect to ρ and using these derived relations. We find

$$K_2 = \frac{1}{\dot{t}}\frac{\partial \dot{p}_\rho}{\partial \rho} = -\frac{1}{2}U^2V''. \tag{B.0.9}$$

Since we now have our expressions for K_1 and K_2 we have found an expression for λ in terms of U:

$$\lambda = \sqrt{-\frac{V''}{2\dot{t}^2}}. \tag{B.0.10}$$

We will now find an expression for V''. We first rewrite the energy relation:

$$\left(\frac{L}{E}\right)^2 = \rho^2U^4. \tag{B.0.11}$$

Here we have made use of the relations $V = E^2$ and $V' = 0$. Differentiating Eq. (B.0.11) with respect to ρ and rearranging terms gives us

$$U' = -\frac{U}{2\rho}. \tag{B.0.12}$$

We now differentiate Eq. (2.5.13) twice with respect to ρ and make use of the relations in Eq. (B.0.11) and Eq. (B.0.12). We find

$$V'' = 2E^2U^4\left(\frac{3U - 4\rho^2U''}{2\rho^2U^5}\right). \tag{B.0.13}$$

For a final step we substitute this relation into Eq. (B.0.10) and make use of Eq. (2.5.21a). We find an expression for the Lyapunov exponent in the $z = 0$ two black hole plane in terms of U:

$$\lambda = \sqrt{\frac{-3U + 4\rho^2U''}{2\rho^2U^5}}\Bigg|_{\rho=\rho_{out}}. \tag{B.0.14}$$

In this relation, ρ_{out} is the radius of the unstable circular orbit as stated in Eq. (3.2.7). By substituting this radius into U and its second derivative we obtain λ as a function of the mass M, resulting in the graph from Figure 9.

This analysis can be extended for the circular orbits in the three black hole meridian plane. The radius of these orbits is given by $r^2 = \rho^2 + z^2$ and is constant. A small drawback of the meridian plane is that r is not one of the coordinates which specify your spacetime. However, ρ and z are. This leads to the configuration $X_i(t) = (\rho, p_\rho, z, p_z)$ for the coordinates and their momenta. As a result we obtain a 4×4 stability matrix:

$$K_{ij} = \frac{1}{\dot{t}} \begin{pmatrix} \frac{\partial \dot{\rho}}{\partial \rho} & \frac{\partial \dot{\rho}}{\partial p_\rho} & \frac{\partial \dot{\rho}}{\partial z} & \frac{\partial \dot{\rho}}{\partial p_z} \\ \frac{\partial \dot{p}_\rho}{\partial \rho} & \frac{\partial \dot{p}_\rho}{\partial p_\rho} & \frac{\partial \dot{p}_\rho}{\partial z} & \frac{\partial \dot{p}_\rho}{\partial p_z} \\ \frac{\partial \dot{z}}{\partial \rho} & \frac{\partial \dot{z}}{\partial p_\rho} & \frac{\partial \dot{z}}{\partial z} & \frac{\partial \dot{z}}{\partial p_z} \\ \frac{\partial \dot{p}_z}{\partial \rho} & \frac{\partial \dot{p}_z}{\partial p_\rho} & \frac{\partial \dot{p}_z}{\partial z} & \frac{\partial \dot{p}_z}{\partial p_z} \end{pmatrix} \tag{B.0.15}$$

We will find an analytic expression for λ by determining the eigenvalues of this matrix.